Extracellular Lipids Accumulate in Human Carotid Arteries as Distinct Three-Dimensional Structures and Have Proinflammatory Properties

Lehti, Satu

2018-02

Lehti , S , Nguyen , S D , Belevich , I , Vihinen , H , Heikkilä , H M , Soliymani , R , Käkelä , R , Saksi , J , Jauhiainen , M , Grabowski , G A , Kummu , O , Hörkkö , S , Baumann , M , Lindsberg , P J , Jokitalo , E , Kovanen , P T & Öörni , K 2018 , ' Extracellular Lipids Accumulate in Human Carotid Arteries as Distinct Three-Dimensional Structures and Have Proinflammatory Properties ' , The American Journal of Pathology , vol. 188 , no. 2 , pp. 525-538 . https://doi.org/10.1016/j.ajpath.2017.09.019

http://hdl.handle.net/10138/311770
https://doi.org/10.1016/j.ajpath.2017.09.019

Accepted Manuscript

Extracellular lipids accumulate in human carotid arteries as distinct three-dimensional structures and have proinflammatory properties

Satu Lehti, Su D. Nguyen, Ilya Belevich, Helena Vihinen, Hanna M. Heikkilä, Rabah Soliymani, Reijo Käkelä, Jani Saksi, Matti Jauhiainen, Gregory A. Grabowski, Outi Kummu, Sohvi Hörkkö, Marc Baumann, Perttu J. Lindsberg, Eija Jokitalo, Petri T. Kovanen, Katariina Öörni

PII: S0002-9440(17)30405-4

DOI: 10.1016/j.ajpath.2017.09.019

Reference: AJPA 2776

To appear in: *The American Journal of Pathology*

Received Date: 12 April 2017

Revised Date: 11 September 2017

Accepted Date: 26 September 2017

Please cite this article as: Lehti S, Nguyen SD, Belevich I, Vihinen H, Heikkilä HM, Soliymani R, Käkelä R, Saksi J, Jauhiainen M, Grabowski GA, Kummu O, Hörkkö S, Baumann M, Lindsberg PJ, Jokitalo E, Kovanen PT, Öörni K, Extracellular lipids accumulate in human carotid arteries as distinct three-dimensional structures and have proinflammatory properties, *The American Journal of Pathology* (2017), doi: 10.1016/j.ajpath.2017.09.019.

Extracellular lipids accumulate in human carotid arteries as distinct three-dimensional structures and have proinflammatory properties

Satu Lehti[1], Su D. Nguyen[1], Ilya Belevich[2], Helena Vihinen[2], Hanna M. Heikkilä[3], Rabah Soliymani[4], Reijo Käkelä[5], Jani Saksi[3], Matti Jauhiainen[6,7], Gregory A. Grabowski[8,9], Outi Kummu[10], Sohvi Hörkkö[10,11], Marc Baumann[4], Perttu J. Lindsberg[3,12], Eija Jokitalo[2], Petri T. Kovanen[1], and Katariina Öörni[1]

[1]Wihuri Research Institute, Haartmaninkatu 8, 00290 Helsinki, Finland

[2]Institute of Biotechnology, Electron Microscopy Unit, University of Helsinki, Helsinki, Finland

[3]Molecular Neurology, Research Programs Unit, Biomedicum Helsinki, University of Helsinki, Helsinki, Finland

[4]Clinical Proteomics Core Facility, Medicum – Biochemistry and Developmental Biology, School of Medicine, University of Helsinki.

[5]Helsinki University Lipidomics Unit, Department of Biosciences, University of Helsinki, Helsinki, Finland

[6]National Institute for Health and Welfare, Helsinki, Finland

[7]Minerva Foundation Institute for Medical Research, Biomedicum Helsinki, Finland

[8]Cincinnati Children's Hospital Medical Center, Cincinnati Ohio

[9]Kiniksa Pharmaceuticals, Ltd, Wellesley, Massachusetts, United States

[10]Medical Microbiology and Immunology, Research Unit of Biomedicine, University of Oulu Oulu, Finland

[11]Medical Research Center and Nordlab Oulu, University Hospital and University of Oulu, Oulu, Finland

[12]Clinical Neurosciences, Neurology, University of Helsinki and Helsinki University Hospital, Haartmaninkatu 8, 00290 Helsinki, Finland

Corresponding author:

Katariina Öörni

Wihuri Research Institute

Atherosclerosis Research Laboratory

Haartmaninkatu 8

00290 Helsinki

FINLAND

Tel. +358 9 681 4133

Fax: +358 9 637 476

Email: kati.oorni@wri.fi

Running title: Extracellular lipids are proinflammatory

Number of figures: 6

Number of supplemental figures: 6

Number of supplemental tables: 1

Number of supplemental videos: 3

Funding: Supported by grants from the Academy of Finland [grant number 265940 to K.Ö], the Finnish Foundation for Cardiovascular Research [S.L. and K.Ö.], and Helsinki University Hospital research funds (EVO) [H.M.H, J.S., and P.J.L.]. I.B., H.V., and E.J. are supported by the Biocenter Finland. Wihuri Research Institute is maintained by the Jenny and Antti Wihuri Foundation.

Disclosures: G.A.G. serves as Chief Scientific Officer of Kiniksa Pharmaceuticals, Ltd (KPL), a privately held biotechnology company. He serves in this capacity under a consulting contract and is not an employee of KPL. He is also a founder, owns stock in KPL, and has stock options from KPL.

KPL is an immunology-based company and is not in the field of lysosomal acid lipase or other lysosomal diseases.

Abstract

Lipid accumulation is a key characteristic of advancing atherosclerotic lesions. Here we analyzed the ultrastructure of the accumulated lipids in endarterectomized human carotid atherosclerotic plaques using three-dimensional (3D) electron microscopy, a method never used in this context before. 3D-electron microscopy revealed intracellular lipid droplets and extracellular lipoprotein particles. The majority of the particles were aggregated and some connected to needle-shaped or sheet-like cholesterol crystals. Proteomic analysis of isolated extracellular lipoprotein particles revealed that apolipoprotein B is their main protein component indicating their origin from low density lipoprotein, intermediate density lipoprotein, very low density lipoprotein, lipoprotein (a), or chylomicron remnants. The particles also contained small exchangeable apolipoproteins, complement components, and immunoglobulins. Lipidomic analysis revealed differences between plasma lipoproteins and the particles thereby indicating involvement of lipolytic enzymes in their generation. Incubation of human monocyte-derived macrophages with the isolated extracellular lipoprotein particles or with plasma lipoproteins that had been lipolytically modified *in vitro* induced intracellular lipid accumulation and triggered inflammasome activation in them. Taken together, extracellular lipids accumulate in human carotid plaques as distinct 3D-structures that include aggregated and fused lipoprotein particles and cholesterol crystals. The particles originate from plasma lipoproteins, show signs of lipolytic modifications and associate with cholesterol crystals. By inducing intracellular cholesterol accumulation (ie, foam cell formation) and inflammasome activation, the extracellular lipoprotein particles may actively enhance atherogenesis.

Introduction

Atherosclerosis underlies carotid artery disease, which is one of the leading causes of ischemic strokes.[1] In carotid arteries, like in other atherosclerosis-susceptible arterial beds, circulating liver-derived apolipoprotein B (apoB)-100–containing and gut-derived apoB-48–containing lipoprotein particles enter the arterial wall,[2] and may so initiate and sustain the development of atherosclerotic lesions. The atherogenic lipoproteins capable of entering arterial intima, the site of atherogenesis, are very low density lipoprotein (VLDL) remnants, low density lipoprotein (LDL) particles, and chylomicron remnants.[3,4] In the intima, the particles bind to extracellular matrix proteoglycans via apoB or apoE.[5-7]

The retained lipoprotein particles are susceptible to a variety of modifications, such as proteolysis, lipolysis, and oxidation,[8] and, indeed, lipoprotein particles isolated from atherosclerotic lesions show signs of these types of modifications.[9-12] Intimal macrophages, mast cells, and smooth muscle cells secrete various proteolytic, lipolytic, and oxidizing enzymes, and biologically active agents, many of which have been shown to be able to attack lipoprotein particles. These include cathepsins,[13-16] matrix metalloproteinases[17], and mast cell chymase[18,19], various forms of phospholipase A_2 (PLA_2), and secreted sphingomyelinase (SMase).[20-24] Importantly, proteolyzed or oxidized LDL particles are more susceptible to lipolytic modifications,[14,20,25] a finding that supports the concept of multiply-modified lipoprotein particles.

Modification of LDL surface changes the conformation of apoB-100.[26,27] Perturbations of the surface phospholipid monolayer also enable efficient hydrolysis of the cholesteryl esters (CE) and triacylglycerols (TAGs) in LDL core, thus causing transformation of LDL particles into liposomes and multilamellar vesicles.[28] Indeed, the presence of cholesteryl esterase–modified LDL has been verified in atherosclerotic lesions.[25] As hydrolysis of CEs leads to the

generation of unesterified cholesterol, the critical concentration of cholesterol may be surpassed, thus allowing nucleation of cholesterol crystals.[29,30]

Surface changes may lead to aggregation of the particles.[8] Aggregated and fused lipoprotein particles have a higher affinity for arterial proteoglycans than monomeric lipoproteins, promoting their retention within the extracellular matrix.[31] In the intima, the modified and aggregated lipoprotein particles can also be taken up by macrophages or smooth muscle cells, which then gradually become foam cells.[32,33] Uptake of modified LDL can also induce nucleation of cholesterol crystals in the lysosomes of the cells.[34] Cholesterol crystals, whether taken up or generated within the lysosomes, have an ability to activate the NLRP3-inflammasome,[35-37] a complex that regulates the generation of active caspase-1, which, again, catalyzes the cleavage of pro–IL-1β and pro–IL-18 into their biologically active secretable forms. The expression of several key inflammasome components has been shown to be increased in atherosclerotic lesions.[38] In addition to cholesterol crystals, also other lipids formed upon LDL modification can induce inflammatory activation of macrophages. Of those lipids, lysophospholipids, and, in presence of glucose, also unesterified fatty acids have been shown to induce IL-1β secretion by macrophages.[39,40]

In this study, the ultrastructure of the lipoprotein particles accumulated in advanced human atherosclerotic lesions was first examined *in situ*. This was conducted by analyzing samples of endarterectomized carotid atherosclerotic plaques by three-dimensional electron microscopy (3D-EM), a method not previously used in this context. The extracellular lipoprotein particles present in the plaques were then isolated and molecularly characterized; they were found to be metabolically relevant lipoprotein-derived structures, which can induce not only lipid-accumulation but also inflammation in atherogenesis.

Materials and Methods

Ethics statement

The use of human material conforms to the principles outlined in the Declaration of Helsinki and the study protocol was approved by the local Medical Ethics Committee. All patients had signed an informed consent document. Human plasma and buffy coats were obtained from healthy blood donors (Finnish Red Cross Blood Service, Helsinki, Finland), who had signed an informed consent document. The plasma samples were by-products from the preparation of blood products for clinical use. The use of the samples was approved by the Finnish Red Cross Blood Service.

Carotid artery samples

Atherosclerotic plaques from human external or common carotid arteries were acquired from patients undergoing carotid endarterectomy operation in the Department of Vascular Surgery of the Helsinki University Hospital. Altogether 322 tissue pieces, one per plaque, from 279 patients, were cut from the endarterectomized carotid plaques, and used in this study. Intimal pieces for immunohistochemistry (four plaques from four patients) or electron microscopy (six plaques from six patients, four of them same as for immunohistochemistry) were fixed and processed immediately after the excision. Pieces intended for lipoprotein particle isolation and consequent analyses were frozen in liquid nitrogen and stored at -80 °C until use.

3D-electron microscopy

The plaque pieces for 3D-EM were fixed with 2% formaldehyde, 2.5% glutaraldehyde, in 0.1 M Na-cacodylate buffer (pH 7.4) supplemented with 2 mM $CaCl_2$ for two to three h. The fixed samples were stored in 0.1 M Na-cacodylate-2 mM $CaCl_2$ buffer containing 2% of

paraformaldehyde for stability and were further processed using a previously described protocol for enhanced contrast.[41,42] Durcupan ACM resin (Merck Sigma-Aldrich Darmstadt, Germany) was mixed according to the manufacturer's recommendations. After dehydration and infiltration, samples were embedded in silicone holders filled with 100% Durcupan and incubated for at least two h before polymerization at 60 °C. A pyramid of tissue was trimmed and mounted on a pin using conductive epoxy glue (CircuitWorks 2400 Kennesaw, GA) for serial block-face electron microscopy (SBEM). Finally, the sides of the pyramid were covered with silver paint (Agar Scientific Ltd. Stansted, UK) and the whole assembly was platinum-coated using Quorum Q150TS (Quorum Technologies, Laughton UK). SBEM datasets were acquired with a FEG-SEM Quanta 250 (FEI; Hillsboro, OR), using a backscattered electron detector (Gatan Inc. Pleasanton, CA) with 2.5-kV beam voltage, spot size 3 and pressure 0.2 Torr. The block faces were cut with 40 nm increments and imaged with XY resolution of 20 nm per pixel.

For electron tomography (ET), semi-thick 250-nm-sections were cut from a trimmed pyramid using a Leica ultracut UCT ultramicrotome and 10-nm colloidal gold particles were placed on top/below the section to serve as fiducial markers for the alignment. The dual axis tilt series was recorded using Tecnai FEG 20 transmission electron microscope (FEI) operating at 200 kV. Images were acquired using SerialEM software[43] and a 4k × 4k Ultrascan 4000 CCD camera (Gatan) at nominal magnification 9,600 ×, providing a 2 × binned pixel size of 1.94 nm. For tilt series, the specimens were tilted at one-degree intervals using a high tilt specimen holder (model 2020; E.A. Fischione Instruments Roskilde, Denmark) between ±62°. The Tilt series were aligned and reconstructed with IMOD software package[44] and the tomographic reconstruction was analyzed, modelled, and visualized with MIB[45] (Version 0.999) and Amira (FEI) (version 6.0.1) software.

Immunohistochemistry

For immunohistochemistry, antigen was retrieved using Tris-EDTA-buffer (pH 9.0, 10 mM Tris, 1 mM EDTA, 0.05 % Tween-20) for 30 minutes in 95 °C water bath, after which the sections were allowed to cool down in the buffer. Paraffin-embedded sections of carotid atherosclerotic plaques were stained for ApoB-100 (a mouse monoclonal anti-apoB antibody LS-C35039, Lifespan Biosciences, Seattle, WA, 1:100 or a polyclonal apoB antibody raised in sheep (1.6 µg/mL of IgG in antiserum of bleed # 20, Sheep L3, THL, Dr M. Jauhiainen, National Institute for Health and Welfare, Finland 1:100)), apoE (Clone WU E-4, Cat, sc-53570, Santa Cruz Biotechnology, USA 1:100), apoA-I (Clone 1C5, Cat. MON5030, Monosan, Netherlands 1:5000), and apoC-III (polyclonal rabbit anti-apoC-III, clone H-75, Cat. sc-50377, Santa Cruz Biotechnology, Dallas, TX, 1:100). The antibodies were detected using DAKO EnVision Kit (Mouse DAB Cat, K4007, DAKO A/S, Denmark), rabbit anti-sheep IgG-HRP (Cat. sc-2770, Santa Cruz Biotechnology, USA, 1:200), or DAKO EnVision+ System HRP (DAB) Rabbit (Cat, K4010, DAKO A/S, Glostrup Denmark), respectively.

Lipoprotein modification and generation of cholesterol crystals

LDL (d = 1.019 to 1.050 g/mL) and VLDL (d < 1.006 g/mL) were isolated from plasma donated by healthy volunteers using sequential ultracentrifugation.[46] The lipoproteins (1 mg/mL) were modified first by PLA_2 (30 U/mL, bee venom PLA_2, (P9279, Sigma Aldrich)), SMase (1000 U/mL, from Bacillus cereus, (S9396, Sigma Aldrich)), α-chymotrypsin (400 U/mL (C4129, Sigma Aldrich)), or 5 µM $CuSO_4$ in PBS containing 2 mM $CaCl_2$ and 2 mM $MgCl_2$. After incubation for 18h at 37 °C, the reactions were stopped by addition of phenyl-methyl sulfonyl fluoride at a final concentration of 0.02 mg/mL (α-chymotrypsin) or the addition of EDTA at a final concentration of 10 mM (PLA_2, SMase, and oxidation). In some

cases the particles were further modified by human recombinant lysosomal acid lipase[47] (LAL) (6 U/µL) in 5 mM in MES - 150 mM NaCl in presence of 2 mmol/L Ca^{2+},100 µmol/L Zn^{2+}, 2 mmol/L Mg^{2+}, at pH 5.0 for 24 to 72 h.[47] Formation of cholesterol crystals was visualized in light microscopy using a polarizing filter. The cholesterol crystals applied to the cells were generated as follows[36]: cholesterol was dissolved in 95% ethanol at a concentration of 12.5 mg/mL at 60 °C, filtered while warm and left to crystallize at 20 °C for four to seven days. Crystals were dried by filtering, ground with a mortar and a pestle in sterile surroundings and kept at -20 °C until used. Endotoxin activity was tested from plasma lipoproteins, isolated extracellular lipoprotein particles, and the dry crystals with endotoxin kit using a kinetic measuring method (Limulus Amebocyte Lysate Pyrogent Plus, (N294-03, Cambrex, Lonza group AG, Basel, Switzerland).

Isolation and analysis of extracellular lipoprotein particles

Plaque pieces were pooled into sets of 10 to 20, each piece from an individual plaque, sets weighing on average 2,500 mg. Extracellular lipoprotein particles were isolated as described previously.[48] Briefly, the snap-frozen tissue was homogenized under liquid nitrogen and lipoprotein particles were extracted first with buffer containing 0.15 M NaCl and thereafter with buffer containing 1.5 M NaCl. The combined extracts were ultracentrifuged for 21 h in SW41Ti rotor (Beckman Coulter, Indianapolis, IN, 40 000 rpm, gmax = 288 000 x g) at a density of 1.063 g/mL after which the lipoprotein particles were collected from the top of the ultracentrifugation tube.

The size distribution of the lipoprotein particles was analyzed using rate zonal ultracentrifugation as described previously.[48] Oxidized epitopes were determined with chemiluminescece immunoassay[48] using mouse monoclonal antibodies recognizing malondialdehyde- and malondialdehyde acetaldehyde epitopes. The sizes of the extracellular

particles were measured using dynamic light scattering (Zetasizer Nano, Malvern Instruments, Malvern Works, Malvern, UK). The cholesterol and triglyceride contents of the lipoprotein particles were measured by a fluorometric Amplex Red cholesterol assay Kit (Cat. A12216, Thermo Fisher Scientific, Waltham, MA) and Triglyceride quantification kit (Cat. K622-100, BioVision, Milpitas, CA), according to manufacturer's instructions.

Western blotting

Isolated extracellular lipoprotein particles, VLDL, LDL, and homogenized plaque tissue (tissue remnants after isolation of the extracellular lipoprotein particles were homogenized in RIPA-buffer using PowerLyzer 24 Bench Top Bead-Based homogenizer using zirconium oxide beads (MO Bio Laboratories (Carlsbad, CA)) were run in 4% to 20% SDS-PAGE gel (165 V 50 min), and transferred onto PVDF (Immobilon Psq, MerckMillipore KGaA, Darmstadt Germany) membrane using wet blot with 20 % methanol in the transfer buffer (200 mA, 60 min). The antibodies used were a polyclonal antibody against apoB-100 (Dr M. Jauhiainen, National Institute for Health and Welfare, Finland) and a respective secondary antibody, rabbit anti-sheep IgG-HRP (Cat.-2770, Santa Cruz Biotechnology, USA 1:2000), a monoclonal antibody against apoE (Clone WU E-4, Cat. sc-53570, Santa Cruz), and a respective goat anti-mouse (DAKO Cat. P0447, polyclonal Goat-anti-mouse HRP), and a guinea pig anti-human polyclonal antibody GP29 against perilipin 1 (Progen Biotechink GmbH, Heidelberg, Germany 1:2000) and a respective secondary antibody, a HRP-conjugated Rabbit anti-Guinea-pig, 1:10000, (Invitrogen, Camarillo, CA).

Lipid mass spectrometry

The lipids were extracted[49] from native LDL and isolated extracellular lipoprotein particles and dried under N_2 flow and dissolved in chloroform/methanol (1:2). The samples were spiked with a mixture of several quantitative standards, and just prior to the analysis 1% (v/v)

of NH_3 was added to each sample to support ionization and prevent adduct formation. The mass spectra indicating all positive ions, all negative ions or precursors of the ion m/z 184 (specific fragment for choline head group) were recorded by Agilent 6490 Triple Quad LC/MS with iFunnel technology (Agilent Technologies, CA). The data were further analyzed with MassHunter (Agilent Technologies) and LIMSA[50] software (Version 1.0), the latter employing the standards and a lipid library.

High-performance thin layer chromatography

Neutral lipid and phospholipid contents were determined using high performance thin layer chromatography. Aliquots (50 µL) of each lipid sample (in chloroform/methanol 1:2) and standards for each lipid class were applied onto silica plates with CAMAG Automatic TLC Sampler 4 (CAMAG, Muttenz, Switzerland). Standard curves were prepared separately for each lipid class. The lipids of the applied samples were separated on the plates by using as eluent hexane/diethyl ether/acetic acid/water (26/6/0.4/0.1) for neutral lipids and chloroform/methanol/acetic acid/water (25/17.5/3.8/1.75) for phospholipids. The plates were developed by dipping them in 3% $CuSO_4 \cdot 5H_2O$ + 8% H_3PO_4 aqueous solution, and heating them on a hot plate until visible sample lines. The lipids were quantified by scanning the plates under ultraviolet (254 nm) light by CAMAG TLC Scanner 3 and integrating the peak areas by winCATS program (CAMAG Version 1.1.3.0).

Circular dichroism

Circular dichroism was used to analyze the protein conformation of the extracellular particles. Samples of native LDL or extracellular particles (50 µg/mL) were analyzed by circular dichroism as described previously[26,51] using a JASCO J-715 spectropolarimeter (Japan Spectroscopic Co.; Tokyo, Japan). For each sample, five spectra were averaged, and blank measurements were subtracted.

Sample preparation and proteolytic digestion of proteins for MS analysis

Ten microgram of total protein amounts from delipidated samples were digested, using modified FASP protocol.[52] The proteins were reduced, iodoacetamide alkylated, and digested in 10 kDa cut off Amicon®-0.5 filter (Millipore, Ireland) with lysine-C endopeptidase (Wako, Richmond, VA) in a ratio of 1:50 w/w in 4M urea, 0.1M ammonium bicarbonate. The peptide digests were collected by centrifugation and the digestion was continued using trypsin in a ratio of 1:50 w/w in 50 mM ammonium bicarbonate at ambient temperature. The peptide digests were collected and combined. The peptides were cleaned using C18 -reverse phase ZipTipTM (Millipore), re-suspended in 1 % TFA and sonicated in water bath for one minute.

Liquid chromatography-high definition mass spectrometry (LC-HDMS^E)

Three-hundred nanogram of digested proteins were injected for liquid chromatography-mass spectrometry (LC-MS) analysis. The peptides were separated by nanoAcquity UPLC system (Waters) equipped with a trapping column 5 µm Symmetry C18 180 µm × 20 mm C18 reverse phase (Waters), followed by an analytical 1.7 µm, 75 µm × 250 mm BEH-130 C18 reversed-phase column (Waters), in a single pump trapping mode. The injected sample analytes were trapped at a flow rate of 15 µL/min in 99.5% of solution A (0.1 % formic acid). After trapping, the peptides were separated with a linear gradient of 3% to 35% of solution B (0.1% formic acid/acetonitrile), for 30 min at a flow rate 0.3 µL/min and stable column temperature of 35 °C. The samples were run in ion mobility data-independent analysis mode (HDMS^E), in a Synapt G2-S mass spectrometer (Waters), by alternating between low collision energy (6V) and high collision energy ramp in the transfer compartment (20 to 45 V) and using 1 sec cycle time. The separated peptides were detected online with mass spectrometer, operated in positive, resolution mode in the range of m/z 50 to 2000 amu. 150

fmol/µL of human [Glu1]-fibrinopeptide B (Sigma Aldrich) in 50% acetonitrile/0.1% formic acid solution at a flow rate of 0.3 µL/min was used for a lock mass correction, applied every 30 sec.

Protein database search

ProteinLynx Global Server software (PLGS V3.0) (Waters) was used for protein identification. MSE parameters were set as follows: low energy threshold of 135 counts, elevated energy threshold of 30 counts, and intensity threshold of precursor/fragment ion cluster 750 counts. Database searches were performed against Homo sapiens UniProtKB-SwissProt, reviewed, database (release 2016_1, 42145 entries) with Ion Accounting algorithm and using the following parameters: peptide and fragment tolerance: automatic, maximum protein mass: 750 kDa, min fragment ions matches per protein ≥ 7, min fragment ions matches per peptide ≥ 3, min peptide matches per protein ≥ 1, primary digest reagent: trypsin, missed cleavages allowed: 2, fixed modification: carbamidomethylation C, variable modifications: deamidation of NQ amino acid residues, oxidation of Methionine (M) and false discovery rate (FDR) < 4%.

Cell culture

Human primary monocytes were isolated from buffy coats obtained from the Finnish Red Cross Blood Service, Helsinki, Finland, and differentiated into macrophages in the presence of 50 ng/mL of macrophage-colony stimulating factor (M-CSF), as described.[36] The cells were used on day 7 of culture. Prior to activation, the cells were primed with 1 µg/mL LPS (Lipopolysaccharides from Escherichia coli 0111:B4, Sigma Aldrich) for four h. Human primary monocyte–derived macrophages were given native and modified LDL particles (0.3 to 0.4 mg/mL of protein), *in vitro* prepared cholesterol crystals (1 mg/mL), and extracellular lipoprotein particles (0.3 mg/mL of protein) isolated from the atherosclerotic lesions. After an

overnight incubation, media was collected for IL-1β-ELISA-analysis. Accumulation of cholesteryl esters in the cells was evaluated by thin layer chromatography. For this purpose cellular lipids were extracted by incubating PBS-washed cells with hexane/isopropanol mixture (3:2). The protein concentrations of the same cells were determined by first disrupting the cells with 0.2 N NaOH, after which the protein concentration was determined using BCA protein Assay Reagent Kit (232225, Pierce Biotechnology, Rockford, IL)

ELISA-assays

IL-1β–levels from the cell culture media were measured with ELISA (Human IL-1β/IL-1F2 DUOSET ELISA kit, Cat. DY201, R & D Systems Oxon, United Kingdom), according to the manufacturer's instructions. ApoB-100 was assessed from the extracellular lipoprotein particles using Human Apolipoprotein B (specific for apoB-100, does not recognize apoB-48) ELISA development kit (Cat. 3715-1A-6), Mabtech, Nacka Strand, Sweden.

Statistical analysis

Statistical analyses were performed using ANOVA on ranks with pair-wise Wilcoxon signed ranks test or the nonparametric Kruskal-Wallis test, available in the software package SPSS statistics version 23 (IBM, Armonk, NY); $P < 0.05$ was considered statistically significant.

Results

Electron microscopic imaging of atherosclerotic lesions

Pieces of plaques derived from six different endarterectomized carotid atherosclerotic plaques were fixed using a mixture of formaldehyde and glutaraldehyde for maximal preservation of morphology. The fixed samples were further contrasted with four heavy metal staining steps prior plastic embedding. In transmission electron microscopy (TEM), foam cells, extracellular lipoprotein particles, and cholesterol crystals were observed. Figure 1A shows an example of a foam cell surrounded by extracellular lipoprotein particles and cholesterol crystals (at higher magnification in Figure 1B). The diameters of the extracellular particles ranged from 50 to 400 nm, whereas intracellular lipid droplets were much larger, their diameters ranging to more than 2000 nm. Supplemental Figure S1 shows a partial cross-section of an atherosclerotic lesion starting from endothelial cells and extending 420 µm in to the intima. The enlargements show a group of large cholesterol crystals in the deep intima (Supplemental Figure S1B), cholesterol crystals inside and next to foam cells (Supplemental figure S1C-D), and very small cholesterol crystals (<0.5 µm) among extracellular lipoprotein particles (Supplemental Figure S1E-F).

A specimen of an atherosclerotic carotid plaque was selected for serial block-face scanning electron microscopy (SB-EM), in which 340 block-faces, each 40 nm apart, were sequentially cut and imaged. The resulting volume was aligned and segmented to generate a 3D model of organization of cholesterol crystals and foam cells (Supplemental video S1). A representative block-face image is shown in Figure 1C. The micrographs acquired by SB-EM revealed three-dimensional cholesterol crystals embedded in lipoprotein particle-containing extracellular matrix. The 3D model generated from SB-EM dataset is shown in Figure 1D and in Supplemental videos S1 and S2. The needle-like crystals appeared to grow out of

exceptionally large extracellular lipoprotein particles, and some crystals appeared as very large sheet-like structures (Figure 1D). One of the foam cells appeared to be in the process of engulfing two cholesterol crystal sheets (Figure 1D; Supplemental video S2). To obtain the 3D organization of the extracellular lipoprotein particles at higher resolution, electron tomography of the same plaque specimen was also performed, which allowed various projection images of a semi-thick section to be collected and reconstructed into a 3D tomographic volume. Using this method, aggregated lipoprotein particles, some of which appeared to be fusing (Figures 1E and 1F, Supplemental video S3) were observed. The diameters of these extracellular particles ranged from 15 to 135 nm indicating that some of the particles are smaller than plasma LDL (20 to 25 nm), whereas some were much larger.

Generation of cholesterol crystals *in vitro*

Hydrolysis of LDL with the combination of SMase and cholesteryl esterase produces cholesterol crystals *in vitro*.[30] This observation and our present electron microscopic demonstration of cholesterol crystals appearing to grow out from extracellular lipoprotein particles prompted us to test whether also other modifications of plasma LDL, such as lipolysis with PLA_2, oxidation, or proteolysis in combination with cholesteryl ester hydrolysis would be able to induce the formation of cholesterol crystals. Cholesterol is known to crystallize when a critical concentration of unesterified cholesterol has been achieved.[53] We hypothesized that cholesterol crystallization would occur when CEs in LDL core are hydrolyzed into UC. Since destabilization of LDL surface significantly improves CE hydrolysis,[13] LDL particles were first treated with α-chymotrypsin, SMase, or PLA_2, or oxidized with $CuSO_4$ to destabilize particle surface, and thereafter the particles were treated with LAL to hydrolyze the CEs in the LDL core. Examination of the modified LDL particles under polarized light showed that each of these modifications and even treatment of LDL

with LAL without any prior modification was able to induce the formation of cholesterol crystals (Supplemental Figure S2).

Characterization of the extracellular lipoprotein particles

Immunohistochemistry of carotid artery plaques showed the presence of apoB, apoE, apoA-I, and apoC-III, reflecting entry LDL and other plasma lipoproteins into the plaques (Supplemental Figure S3). To gain information of the origins and effects of the lipoprotein-derived lipid particles, extracellular particles from plaques were next isolated and analyzed using a method optimized for this purpose.[48] Pieces of 10 to 20 individual plaques were pooled for each lipoprotein particle isolation. The isolated extracellular lipoprotein particles were found to contain apoB-100, as demonstrated when analyzing them by chemiluminescent immunoassay (Supplemental Figure S4A) or Western blotting (Supplemental Figure S4B). In addition, apoE was detected in the extracellular lipoprotein particles by Western blotting (Supplemental Figure S4B). A more detailed proteomic analysis of extracellular lipoprotein particles by mass spectrometry confirmed the presence of apoB-100 and apoE, and indicated also the presence of other apolipoproteins, such as apoA-I and apoC-III, as well as complement components C3 and C9 and immunoglobulins IgG, IgM, and IgA (Supplemental Table S1). Markers of intracellular lipid droplets, such as perilipin were not detected in the isolated particles, whereas in the homogenized tissue perilipin was abundant (Supplemental Figure S4C).

The extracellular lipoprotein particles contained epitopes recognized by antibodies generated against malondialdehyde-LDL and malondialdehyde acetaldehyde-LDL, indicating their oxidative modification (Figure 2A). Circular dichroism analysis indicated that the conformation of the proteins in the isolated extracellular lipoprotein particles differed from that in LDL particles and that their α-helical content was much lower than that in plasma

LDL (Figure 2B). The extracellular lipoprotein preparations were found to contain cholesterol crystals (Fig. 2C). The proportions of PC and CE were lower and the proportion of free fatty acids higher than in LDL particles (Figure 2D) suggesting that the extracellular lipoproteins had undergone also lipolysis. The higher proportion of protein in the particles compared with plasma LDL points to the same, but may also be indicative of the extracellular lipoprotein particles containing several different proteins, as described above. The low PC content of the particles was reflected in a decrease in the proportion of a major PC species 34:2 (Supplemental Figure S5A). Changes in the lysophosphatidylcholine and sphingomyelin species were more subtle (Supplemental Figure S4B and C, respectively). The CE composition of the extracellular lipoprotein particles differed from that of plasma LDL. Thus, although the proportion of CE 18:2, the most common CE in LDL, was dramatically lower in the extracellular lipoprotein particles, they had a high but varying proportion of CE 18:3 (Supplemental Figure S6).

Dynamic light scattering analysis revealed that the isolated extracellular lipoprotein particles were much larger (40 to 1000 nm) than plasma LDL (average diameter 24 nm) or VLDL (average diameter 58 nm) (Figure 3A). The extracellular lipoproteins had a wide size distribution also when analyzed using rate zonal ultracentrifugation (Figure 3B and 3C). Cholesterol was distributed among the small and large particles, whereas TG was found only in the largest particles (Figure 3B). ApoE and ApoA-I were found only in the small particles, and their molar concentrations were much lower than that of apoB-100. Immunoreactive apoB-100 was found mainly in the small particles. In this assay, an antibody against a C-terminal epitope is used. As this epitope is not present in apoB-48, the finding suggests the larger particles may be derived from apoB-48-containing particles or that apoB-100 in the large particles had been partially lost or modified (Fig 3C).

Proinflammatory activity of isolated extracellular lipoprotein particles

Cholesterol crystals are a known activator of the NLRP3 inflammasome, an inflammatory pathway that leads to activation of caspase-1 and to secretion of caspase 1–activated IL-1β and IL-18.[35,36] To study whether the isolated extracellular lipoprotein particles are able to induce inflammasome activation, monocyte-derived macrophages were incubated with or without 1 μg/mL of LPS, after which the cells were further incubated in the presence of the lipoprotein particle preparations or, as a positive control, *in vitro* generated cholesterol crystals. In the primary human monocyte-derived macrophages, LPS induces transcription of *NLRP3* and *IL1B*, and thereby serves as a necessary priming signal for inflammasome activation and IL-1β secretion.[54] The lipoprotein particle preparations and cholesterol crystals induced secretion of IL-1β in LPS-primed, but not in non-primed human macrophages (Figure 4A). In the non-primed macrophages, the lipoprotein particle preparations, similar to *in vitro*–generated cholesterol crystals,[36] did not induce significant expression of *NLRP3 or TNFA*, nor did they induce expression of *MCP1* (not shown).

To test whether modified lipoproteins were able to induce IL-1β secretion and activation of inflammasome complexes similar to the isolated lipoprotein particle preparations, LDL surface phospholipids and proteins were first modified using either proteolysis, lipolysis, or oxidation of the particles, after which the core CEs were hydrolyzed by LAL. All these modifications induced formation of cholesterol crystals (Supplemental Figure S2). LDL hydrolyzed with a combination of PLA_2 and LAL induced a robust IL-1β secretion (Figure 4B), but unexpectedly, neither oxidized LDL nor oxidized LDL treated with LAL was able to induce IL-1β secretion by the human macrophages. Similar to LDL modified with PLA_2 and LAL, also VLDL modified by the same enzymes induced secretion of IL-1β (Figure 4C). Secretion of IL-1β could be inhibited by a caspase-1-inhibitor thereby confirming that it was

inflammasome-dependent (Figure 4D). Also, inhibition of uptake of the extracellular lipoprotein particles or modified LDL with cytochalasin D partly inhibited IL-1β secretion (Figure 4D). The isolated extracellular lipoproteins, VLDL (both native and lipolyzed with PLA_2 and LAL), LDL lipolyzed with PLA_2 and LAL, and cholesterol crystals, all were able to induce CE accumulation in the cells, but there were marked compositional differences between the differently treated cells (Figure 5). Thus, cholesterol crystals and modified LDL induced accumulation of CEs, whereas the extracellular lipoprotein particles and native and lipolyzed VLDL induced particularly the accumulation of TAGs. Cholesterol crystals induced also accumulation of UC.

Discussion

To understand the origin of lipid accumulating in atherosclerotic plaques and their pathophysiological significance in human atherogenesis, we assessed the ultrastructure, chemical composition, and proinflammatory potential of lipoprotein particles isolated from endarterectomized carotid artery plaques. We demonstrate that the extracellular lipoprotein particles are derived from modified apoB-containing plasma lipoproteins and when these particles were added to cultured human monocyte-derived macrophages, they triggered proinflammatory activation of macrophages and induced lipid accumulation in the cells *in vitro*. 3D-EM of the plaques revealed areas where the extracellularly located lipoprotein particles, foam cells, and cholesterol crystals were co-localized.

ApoB-100 was found to be the main protein component of the isolated extracellular lipoprotein particles, indicating that the particles were derived from the atherogenic class of plasma lipoproteins containing this apolipoprotein. In addition, chylomicron remnants, another likely source of plasma-derived plaque lipids, also contribute to the accumulating extracellular lipids in the carotid plaques. Mass spectrometric analysis of the particle proteins

confirmed the presence of several small exchangeable apolipoproteins, including apoE, apoA-I, apoC-I, and C-III, which are known to be present in all major lipoprotein classes.[55,56] The extracellular lipoprotein particles contained also complement components, which have been detected in plasma HDL particles.[57] Moreover, immunoglobulins were found to be associated with the extracellular lipoprotein particles, a finding suggesting local formation of immunocomplexes, such as have been reported for oxidized LDL in human atherosclerotic lesions.[58] The isolated particles did not contain markers of intracellular lipid droplets, such as perilipin. The apolipoprotein composition of the extracellular lipoproteins suggests that they are derived from multiple classes of plasma lipoproteins from chylomicron remnants to HDL particles. As apoE is secreted by macrophages[59], it is also possible that this protein as well as complement components and immunoglobulins are be incorporated into the extracellular lipoproteins in the tissue.

Circular dichroism analysis indicated that the protein components of the isolated lipoprotein particles had largely lost their secondary structure. This may have resulted from degradation of the protein components or, also from lipolytic modifications since lipolytic modifications of plasma lipoproteins have been reported to compromise the conformation of their apolipoproteins.[26,60] Indeed, when compared to native LDL particles, the lipid composition of the isolated lipoprotein particles suggested that they had been exposed to the action of both phospholipases and cholesteryl esterases. Their low CE and PC content, as well as decreased PC/SM ratio are also in accordance with previously published results.[12,61,62] Compared to the PC species profile of LDL, the lipoprotein particles were enriched with oxidation-resistant saturated and monounsaturated species, and also with arachidonic acid–containing species with a proinflammatory potential (eg, PC 38:4, acyl pair 18:0/20:4n-6).

The lipoprotein particle preparations were also found to contain cholesterol crystals. Importantly, hydrolysis of CEs in the core of plasma lipoprotein particles can induce

formation of cholesterol crystals, as previously shown by Guarino and co-workers by producing cholesterol crystals by hydrolysis of LDL with SMase and cholesteryl esterase.[30] Here, we show that modification of the surface of LDL particles by proteolysis, phospholipolysis, or oxidation facilitates effective CE hydrolysis leading to induction of cholesterol crystal formation. These modifications have also been shown to induce aggregation and fusion of plasma LDL particles,[8] findings compatible with our present electron microscopic observations of aggregated and fused lipoprotein particles in carotid atherosclerotic plaques

Various electron microscopic techniques (SEM and TEM) have been previously used to image foam cells and extracellular lipoprotein particles in atherosclerotic plaques derived from animals[63-65] or humans.[66-68] Interestingly, freeze-fracturing combined with SEM has provided images of the lipid particles and of their lamellar structure.[65,69] In this study, we used two complementary EM techniques, electron tomography, which allowed us to detect individual lipoprotein particles even in their fusion process, and SB-EM, which allowed observation of cholesterol crystals, extracellular lipoprotein particles, and foam cells within an atherosclerotic plaque. These techniques made it possible to examine the 3D structure of the plaque microdomains and thus to uncover novel information of the positioning and nature of the extracellular lipoprotein particles and cholesterol crystals in the intima. Models generated from SB-EM dataset revealed sheet-like cholesterol crystals that were as large as the neighboring foam cells, as well as needle-like crystals that were connected to extracellular particles and seemingly growing out of them. Such large sheet-like crystals have not been observed in atherosclerotic plaques with any other EM-technique. The sheet-like crystals represent likely late stage forms of the cholesterol crystallization process, which, as shown in bile, evolve from needle-like structures. [70]

Interestingly, in the model generated from the SB-EM dataset, one of the plaque foam cells appeared to be in the process of phagocytosing cholesterol crystals. Uptake of cholesterol crystals by cultured macrophages has been found to activate the NLRP3-inflammasome in them.[35,36] Inflammasome activation is a two-step process, in which the first step, the priming, is induced, eg, by LPS[71], and leads to induction of transcription of *NLRP3*, *CASP1*, and *IL1B*, ie, to the generation of the machinery required for secretion of mature IL-1β. A potential source of LPS in atherosclerotic lesions are oral pathogens.[72] Other priming components include components of the extracellular matrix, such as biglycan, that can interact with Toll-like receptors[73]. In the second step, assembly and activation of the inflammasome complex is triggered by inflammasome activators, such as cholesterol crystals. In this study, we show that the plaque-derived lipoprotein particles are able to trigger inflammasome activation in LPS-primed macrophages. Cytochalasin D induced a partial reduction in the secretion of IL-1β, indicating that the process was at least partly dependent on the internalization of the lipoprotein particles. The lipoprotein particle preparations contained cholesterol crystals rendering it possible that the observed inflammasome activation in the cultured human macrophages was caused solely by them. However, of all types of LDL modifications that induced the formation of cholesterol crystals, only those involving hydrolysis of both PCs and CEs were able to trigger robust IL-1β secretion in cultured human macrophages.

This study demonstrates that the aggregated and fused extracellular lipoprotein particles present in human atherosclerotic lesions are derived mainly from apoB-containing plasma lipoproteins and that they have undergone modifications able to induce lipoprotein aggregation as well as formation of cholesterol crystals (Figure 6). The extracellular lipoprotein particle preparations induced inflammasome activation, and, therefore, the particles can be considered active inflammatory contributors in atherogenesis. Considering that IL-1β, a product of inflammasome activation, is able to induce secretion of matrix

metalloproteinase-1, an enzyme with collagenase activity,[74,75] lipoprotein particle–induced inflammasome activation may also lead to weakening and rupture of an atherosclerotic plaque, and so contribute to the development of atherothrombotic complications. Moreover, as inflammasome activation has been shown to induce cell death by apoptosis and pyroptosis,[76] uptake of extracellular lipoprotein particles may also contribute to death of intimal cells, and, like cholesterol crystals, associate with plaque vulnerability.[77] Thus, plasma lipoproteins retained and modified in the arterial intima can induce both lipid accumulation and inflammation, two key processes that are involved in the formation and progression of atherosclerosis. Finally, multidimensional imaging of the extracellular lipoprotein particles in their genuine environment, ie, in a human atherosclerotic plaque, allows us to better define the ultrastructural architecture of human atherosclerotic lesions, and so aids in understanding of the detailed structure-function relationships of the lipid components in atherogenesis.

Limitations of the study

The method used for isolation of the extracellular lipoprotein particles is a compromise in that the homogenization needs to be sensitive enough to avoid breaking of the foam cells with ensuing release of their intracellular lipid droplets or causing artificial aggregation of the extracellular particles; yet, the homogenization needs to be efficient enough to be able to liberate lipid particles as much as possible. As we did not observe markers of intracellular lipid droplets in the proteomic analysis of the isolated particles, the presence of at least sizeable amounts of lipid droplets of intracellular origin among extracellular particles seems highly unlikely. Intracellular lipid droplets would also have been detected by their large size in the dynamic light scattering analysis and the rate zonal ultracentrifugation.[48] A D_2O-based ultracentrifugation was chosen during the isolation procedure, which is known to minimize the loss of small exchangeable apolipoproteins during the ultracentrifugation step. [55] Also

apoB-100 immunoaffinity columns were not selected to avoid examining only apolipoprotein–pre-specified particles, eg, only apoB-100 –containing particles.

Acknowledgments

We thank Maija Atuegwu, Sirpa Rannikko, Sonja Kasari, Jaana Kautto, Sanna Sihvo, Antti Salminen, and Mervi Lindman for their excellent technical assistance.

References

1. Grotta JC: Carotid stenosis, N Engl J Med 2013, 369:2360-2361

2. Nielsen LB, Gronholdt ML, Schroeder TV, Stender S, Nordestgaard BG: In vivo transfer of lipoprotein(a) into human atherosclerotic carotid arterial intima, Arterioscler Thromb Vasc Biol 1997, 17:905-911

3. Nielsen LB: Transfer of low density lipoprotein into the arterial wall and risk of atherosclerosis, Atherosclerosis 1996, 123:1-15

4. Chapman MJ, Ginsberg HN, Amarenco P, Andreotti F, Boren J, Catapano AL, Descamps OS, Fisher E, Kovanen PT, Kuivenhoven JA, Lesnik P, Masana L, Nordestgaard BG, Ray KK, Reiner Z, Taskinen MR, Tokgozoglu L, Tybjaerg-Hansen A, Watts GF: Triglyceride-rich lipoproteins and high-density lipoprotein cholesterol in patients at high risk of cardiovascular disease: evidence and guidance for management, Eur Heart J 2011, 32:1345-1361

5. Boren J, Olin K, Lee I, Chait A, Wight TN, Innerarity TL: Identification of the principal proteoglycan-binding site in LDL. A single-point mutation in apo-B100 severely affects proteoglycan interaction without affecting LDL receptor binding, J Clin Invest 1998, 101:2658-2664

6. Camejo G, Olsson U, Hurt-Camejo E, Baharamian N, Bondjers G: The extracellular matrix on atherogenesis and diabetes-associated vascular disease, Atheroscler Suppl 2002, 3:3-9

7. O'Brien KD, Olin KL, Alpers CE, Chiu W, Ferguson M, Hudkins K, Wight TN, Chait A: Comparison of apolipoprotein and proteoglycan deposits in human coronary atherosclerotic plaques: colocalization of biglycan with apolipoproteins, Circulation 1998, 98:519-527

8. Öörni K, Pentikäinen MO, Ala-Korpela M, Kovanen PT: Aggregation, fusion, and vesicle formation of modified low density lipoprotein particles: molecular mechanisms and effects on matrix interactions, J Lipid Res 2000, 41:1703-1714

9. Hoff HF, Gaubatz JW: Isolation, purification, and characterization of a lipoprotein containing Apo B from the human aorta, Atherosclerosis 1982, 42:273-297

10. Ylä-Herttuala S, Palinski W, Rosenfeld ME, Steinberg D, Witztum JL: Lipoproteins in normal and atherosclerotic aorta, Eur Heart J 1990, 11 Suppl E:88-99

11. Smith EB, Evans PH, Downham MD: Lipid in the aortic intima. The correlation of morphological and chemical characteristics, J Atheroscler Res 1967, 7:171-186

12. Smith EB, Slater RS, Chu PK: The lipids in raised fatty and fibrous lesions in human aorta. A comparison of the changes at different stages of development, J Atheroscler Res 1968, 8:399-419

13. Hakala JK, Oksjoki R, Laine P, Du H, Grabowski GA, Kovanen PT, Pentikäinen MO: Lysosomal enzymes are released from cultured human macrophages, hydrolyze LDL in vitro, and are present extracellularly in human atherosclerotic lesions, Arterioscler Thromb Vasc Biol 2003, 23:1430-1436

14. Plihtari R, Hurt-Camejo E, Öörni K, Kovanen PT: Proteolysis sensitizes LDL particles to phospholipolysis by secretory phospholipase A2 group V and secretory sphingomyelinase, J Lipid Res 2010, 51:1801-1809

15. Wang J, Sjoberg S, Tang TT, Öörni K, Wu W, Liu C, Secco B, Tia V, Sukhova GK, Fernandes C, Lesner A, Kovanen PT, Libby P, Cheng X, Shi GP: Cathepsin G activity lowers plasma LDL and reduces atherosclerosis, Biochim Biophys Acta 2014, 1842:2174-2183

16. Öörni K, Sneck M, Brömme D, Pentikäinen MO, Lindstedt KA, Mäyranpää M, Aitio H, Kovanen PT: Cysteine protease cathepsin F is expressed in human atherosclerotic lesions,

is secreted by cultured macrophages, and modifies low density lipoprotein particles in vitro, J Biol Chem 2004, 279:34776-34784

17. Edelstein C, Nakajima K, Pfaffinger D, Scanu AM: Oxidative events cause degradation of apoB-100 but not of apo[a] and facilitate enzymatic cleavage of both proteins, J Lipid Res 2001, 42:1664-1670

18. Kokkonen JO, Vartiainen M, Kovanen PT: Low density lipoprotein degradation by secretory granules of rat mast cells. Sequential degradation of apolipoprotein B by granule chymase and carboxypeptidase A, J Biol Chem 1986, 261:16067-16072

19. Kokkonen JO, Kovanen PT: Proteolytic enzymes of mast cell granules degrade low density lipoproteins and promote their granule-mediated uptake by macrophages in vitro, J Biol Chem 1989, 264:10749-10755

20. Schissel SL, Jiang X, Tweedie-Hardman J, Jeong T, Camejo EH, Najib J, Rapp JH, Williams KJ, Tabas I: Secretory sphingomyelinase, a product of the acid sphingomyelinase gene, can hydrolyze atherogenic lipoproteins at neutral pH. Implications for atherosclerotic lesion development, J Biol Chem 1998, 273:2738-2746

21. Sato H, Kato R, Isogai Y, Saka G, Ohtsuki M, Taketomi Y, Yamamoto K, Tsutsumi K, Yamada J, Masuda S, Ishikawa Y, Ishii T, Kobayashi T, Ikeda K, Taguchi R, Hatakeyama S, Hara S, Kudo I, Itabe H, Murakami M: Analyses of group III secreted phospholipase A2 transgenic mice reveal potential participation of this enzyme in plasma lipoprotein modification, macrophage foam cell formation, and atherosclerosis, J Biol Chem 2008, 283:33483-33497

22. Bostrom MA, Boyanovsky BB, Jordan CT, Wadsworth MP, Taatjes DJ, de Beer FC, Webb NR: Group v secretory phospholipase A2 promotes atherosclerosis: evidence from genetically altered mice, Arterioscler Thromb Vasc Biol 2007, 27:600-606

23. Webb NR, Bostrom MA, Szilvassy SJ, van der Westhuyzen DR, Daugherty A, de Beer FC: Macrophage-expressed group IIA secretory phospholipase A2 increases atherosclerotic lesion formation in LDL receptor-deficient mice, Arterioscler Thromb Vasc Biol 2003, 23:263-268

24. Sartipy P, Johansen B, Camejo G, Rosengren B, Bondjers G, Hurt-Camejo E: Binding of human phospholipase A2 type II to proteoglycans. Differential effect of glycosaminoglycans on enzyme activity, J Biol Chem 1996, 271:26307-26314

25. Torzewski M, Suriyaphol P, Paprotka K, Spath L, Ochsenhirt V, Schmitt A, Han SR, Husmann M, Gerl VB, Bhakdi S, Lackner KJ: Enzymatic modification of low-density lipoprotein in the arterial wall: a new role for plasmin and matrix metalloproteinases in atherogenesis, Arterioscler Thromb Vasc Biol 2004, 24:2130-2136

26. Sneck M, Nguyen SD, Pihlajamaa T, Yohannes G, Riekkola ML, Milne R, Kovanen PT, Oorni K: Conformational changes of apoB-100 in SMase-modified LDL mediate formation of large aggregates at acidic pH, J Lipid Res 2012, 53:1832-1839

27. Flood C, Gustafsson M, Pitas RE, Arnaboldi L, Walzem RL, Boren J: Molecular mechanism for changes in proteoglycan binding on compositional changes of the core and the surface of low-density lipoprotein-containing human apolipoprotein B100, Arterioscler Thromb Vasc Biol 2004, 24:564-570

28. Chao FF, Blanchette-Mackie EJ, Tertov VV, Skarlatos SI, Chen YJ, Kruth HS: Hydrolysis of cholesteryl ester in low density lipoprotein converts this lipoprotein to a liposome, J Biol Chem 1992, 267:4992-4998

29. Guarino AJ, Tulenko TN, Wrenn SP: Sphingomyelinase-to-LDL molar ratio determines low density lipoprotein aggregation size: biological significance, Chem Phys Lipids 2006, 142:33-42

30. Guarino AJ, Tulenko TN, Wrenn SP: Cholesterol crystal nucleation from enzymatically modified low-density lipoproteins: combined effect of sphingomyelinase and cholesterol esterase, Biochemistry 2004, 43:1685-1693

31. Öörni K, Posio P, Ala-Korpela M, Jauhiainen M, Kovanen PT: Sphingomyelinase induces aggregation and fusion of small very low-density lipoprotein and intermediate-density lipoprotein particles and increases their retention to human arterial proteoglycans, Arterioscler Thromb Vasc Biol 2005, 25:1678-1683

32. Grosheva I, Haka AS, Qin C, Pierini LM, Maxfield FR: Aggregated LDL in contact with macrophages induces local increases in free cholesterol levels that regulate local actin polymerization, Arterioscler Thromb Vasc Biol 2009, 29:1615-1621

33. Allahverdian S, Pannu PS, Francis GA: Contribution of monocyte-derived macrophages and smooth muscle cells to arterial foam cell formation, Cardiovasc Res 2012, 95:165-172

34. Singh RK, Barbosa-Lorenzi VC, Lund FW, Grosheva I, Maxfield FR, Haka AS: Degradation of aggregated LDL occurs in complex extracellular sub-compartments of the lysosomal synapse, J Cell Sci 2016, 129:1072-1082

35. Duewell P, Kono H, Rayner KJ, Sirois CM, Vladimer G, Bauernfeind FG, Abela GS, Franchi L, Nunez G, Schnurr M, Espevik T, Lien E, Fitzgerald KA, Rock KL, Moore KJ, Wright SD, Hornung V, Latz E: NLRP3 inflammasomes are required for atherogenesis and activated by cholesterol crystals, Nature 2010, 464:1357-1361

36. Rajamäki K, Lappalainen J, Öörni K, Välimäki E, Matikainen S, Kovanen PT, Eklund KK: Cholesterol crystals activate the NLRP3 inflammasome in human macrophages: a novel link between cholesterol metabolism and inflammation, PLoS One 2010, 5:e11765

37. Estruch M, Rajamäki K, Sanchez-Quesada JL, Kovanen PT, Öörni K, Benitez S, Ordonez-Llanos J: Electronegative LDL induces priming and inflammasome activation

leading to IL-1beta release in human monocytes and macrophages, Biochim Biophys Acta 2015, 1851:1442-1449

38. Rajamäki K, Mäyränpää MI, Risco A, Tuimala J, Nurmi K, Cuenda A, Eklund KK, Öörni K, Kovanen PT: p38delta MAPK: A Novel Regulator of NLRP3 Inflammasome Activation With Increased Expression in Coronary Atherogenesis, Arterioscler Thromb Vasc Biol 2016, 36:1937-1946

39. Liu-Wu Y, Hurt-Camejo E, Wiklund O: Lysophosphatidylcholine induces the production of IL-1beta by human monocytes, Atherosclerosis 1998, 137:351-357

40. Dasu MR, Jialal I: Free fatty acids in the presence of high glucose amplify monocyte inflammation via Toll-like receptors, Am J Physiol Endocrinol Metab 2011, 300:E145-154

41. Deerinck TJ, Bushong, E., Thor, A., Ellisman, M.H.: NCMIR methods for 3D EM: A new protocol for preparation of biological specimens for serial block-face SEM, Microscopy 6-8 2010,

42. Kremer A, Lippens S, Bartunkova S, Asselbergh B, Blanpain C, Fendrych M, Goossens A, Holt M, Janssens S, Krols M, Larsimont JC, Mc Guire C, Nowack MK, Saelens X, Schertel A, Schepens B, Slezak M, Timmerman V, Theunis C, R VANB, Visser Y, Guerin CJ: Developing 3D SEM in a broad biological context, J Microsc 2015, 259:80-96

43. Mastronarde DN: Automated electron microscope tomography using robust prediction of specimen movements, J Struct Biol 2005, 152:36-51

44. Kremer JR, Mastronarde DN, McIntosh JR: Computer visualization of three-dimensional image data using IMOD, J Struct Biol 1996, 116:71-76

45. Belevich I, Joensuu M, Kumar D, Vihinen H, Jokitalo E: Microscopy Image Browser: A Platform for Segmentation and Analysis of Multidimensional Datasets, PLoS Biol 2016, 14:e1002340

46. Radding CM, Steinberg D: Studies on the synthesis and secretion of serum lipoproteins by rat liver slices, J Clin Invest 1960, 39:1560-1569

47. Sun Y, Xu YH, Du H, Quinn B, Liou B, Stanton L, Inskeep V, Ran H, Jakubowitz P, Grilliot N, Grabowski GA: Reversal of advanced disease in lysosomal acid lipase deficient mice: a model for lysosomal acid lipase deficiency disease, Mol Genet Metab 2014, 112:229-241

48. Lehti S, Käkelä R., Hörkkö, S., Kummu, O., Helske-Suihko, S., Kupari, M., Werkkala, K., Kovanen, P.T., Öörni, K.: Modified lipoprotein-derived lipid particles accumulate in human stenotic aortic valves, PLoS ONE 2013,

49. Folch J, Lees M, Sloane Stanley GH: A simple method for the isolation and purification of total lipides from animal tissues, J Biol Chem 1957, 226:497-509

50. Haimi P, Uphoff A, Hermansson M, Somerharju P: Software tools for analysis of mass spectrometric lipidome data, Anal Chem 2006, 78:8324-8331

51. Nguyen SD, Öörni K, Lee-Rueckert M, Pihlajamaa T, Metso J, Jauhiainen M, Kovanen PT: Spontaneous remodeling of HDL particles at acidic pH enhances their capacity to induce cholesterol efflux from human macrophage foam cells, J Lipid Res 2012, 53:2115-2125

52. Scifo E, Szwajda A, Soliymani R, Pezzini F, Bianchi M, Dapkunas A, Debski J, Uusi-Rauva K, Dadlez M, Gingras AC, Tyynela J, Simonati A, Jalanko A, Baumann MH, Lalowski M: Proteomic analysis of the palmitoyl protein thioesterase 1 interactome in SH-SY5Y human neuroblastoma cells, J Proteomics 2015, 123:42-53

53. Katz SS, Shipley GG, Small DM: Physical chemistry of the lipids of human atherosclerotic lesions. Demonstration of a lesion intermediate between fatty streaks and advanced plaques, J Clin Invest 1976, 58:200-211

54. Bauernfeind FG, Horvath G, Stutz A, Alnemri ES, MacDonald K, Speert D, Fernandes-Alnemri T, Wu J, Monks BG, Fitzgerald KA, Hornung V, Latz E: Cutting edge: NF-kappaB activating pattern recognition and cytokine receptors license NLRP3 inflammasome activation by regulating NLRP3 expression, J Immunol 2009, 183:787-791

55. Ståhlman M, Davidsson P, Kanmert I, Rosengren B, Boren J, Fagerberg B, Camejo G: Proteomics and lipids of lipoproteins isolated at low salt concentrations in D2O/sucrose or in KBr, J Lipid Res 2008, 49:481-490

56. Davidsson P, Hulthe J, Fagerberg B, Camejo G: Proteomics of apolipoproteins and associated proteins from plasma high-density lipoproteins, Arterioscler Thromb Vasc Biol 2010, 30:156-163

57. Vaisar T, Pennathur S, Green PS, Gharib SA, Hoofnagle AN, Cheung MC, Byun J, Vuletic S, Kassim S, Singh P, Chea H, Knopp RH, Brunzell J, Geary R, Chait A, Zhao XQ, Elkon K, Marcovina S, Ridker P, Oram JF, Heinecke JW: Shotgun proteomics implicates protease inhibition and complement activation in the antiinflammatory properties of HDL, J Clin Invest 2007, 117:746-756

58. Ylä-Herttuala S, Palinski W, Butler SW, Picard S, Steinberg D, Witztum JL: Rabbit and human atherosclerotic lesions contain IgG that recognizes epitopes of oxidized LDL, Arterioscler Thromb 1994, 14:32-40

59. Kockx M, Jessup W, Kritharides L: Regulation of endogenous apolipoprotein E secretion by macrophages, Arterioscler Thromb Vasc Biol 2008, 28:1060-1067

60. Asatryan L, Hamilton RT, Isas JM, Hwang J, Kayed R, Sevanian A: LDL phospholipid hydrolysis produces modified electronegative particles with an unfolded apoB-100 protein, J Lipid Res 2005, 46:115-122

61. Chao FF, Blanchette-Mackie EJ, Chen YJ, Dickens BF, Berlin E, Amende LM, Skarlatos SI, Gamble W, Resau JH, Mergner WT, et al.: Characterization of two unique

cholesterol-rich lipid particles isolated from human atherosclerotic lesions, Am J Pathol 1990, 136:169-179

62. Tailleux A, Torpier G, Caron B, Fruchart JC, Fievet C: Immunological properties of apoB-containing lipoprotein particles in human atherosclerotic arteries, J Lipid Res 1993, 34:719-728

63. Simionescu N, Vasile E, Lupu F, Popescu G, Simionescu M: Prelesional events in atherogenesis. Accumulation of extracellular cholesterol-rich liposomes in the arterial intima and cardiac valves of the hyperlipidemic rabbit, Am J Pathol 1986, 123:109-125

64. Filip DA, Nistor A, Bulla A, Radu A, Lupu F, Simionescu M: Cellular events in the development of valvular atherosclerotic lesions induced by experimental hypercholesterolemia, Atherosclerosis 1987, 67:199-214

65. Nievelstein PF, Fogelman AM, Mottino G, Frank JS: Lipid accumulation in rabbit aortic intima 2 hours after bolus infusion of low density lipoprotein. A deep-etch and immunolocalization study of ultrarapidly frozen tissue, Arterioscler Thromb 1991, 11:1795-1805

66. Bocan TM, Schifani TA, Guyton JR: Ultrastructure of the human aortic fibrolipid lesion. Formation of the atherosclerotic lipid-rich core, Am J Pathol 1986, 123:413-424

67. Pasquinelli G, Preda P, Vici M, Gargiulo M, Stella A, D'Addato M, Laschi R: Electron microscopy of lipid deposits in human atherosclerosis, Scanning Microsc 1989, 3:1151-1159

68. Guyton JR, Klemp KF: The lipid-rich core region of human atherosclerotic fibrous plaques. Prevalence of small lipid droplets and vesicles by electron microscopy, Am J Pathol 1989, 134:705-717

69. Lupu F, Danaricu I, Simionescu N: Development of intracellular lipid deposits in the lipid-laden cells of atherosclerotic lesions. A cytochemical and ultrastructural study, Atherosclerosis 1987, 67:127-142

70. Konikoff FM, Chung DS, Donovan JM, Small DM, Carey MC: Filamentous, helical, and tubular microstructures during cholesterol crystallization from bile. Evidence that cholesterol does not nucleate classic monohydrate plates, J Clin Invest 1992, 90:1155-1160

71. Mani V, Hollis JH, Gabler NK: Dietary oil composition differentially modulates intestinal endotoxin transport and postprandial endotoxemia, Nutr Metab (Lond) 2013, 10:6

72. Kozarov EV, Dorn BR, Shelburne CE, Dunn WA, Jr., Progulske-Fox A: Human atherosclerotic plaque contains viable invasive Actinobacillus actinomycetemcomitans and Porphyromonas gingivalis, Arterioscler Thromb Vasc Biol 2005, 25:e17-18

73. Babelova A, Moreth K, Tsalastra-Greul W, Zeng-Brouwers J, Eickelberg O, Young MF, Bruckner P, Pfeilschifter J, Schaefer RM, Grone HJ, Schaefer L: Biglycan, a danger signal that activates the NLRP3 inflammasome via toll-like and P2X receptors, J Biol Chem 2009, 284:24035-24048

74. Tsuzaki M, Guyton G, Garrett W, Archambault JM, Herzog W, Almekinders L, Bynum D, Yang X, Banes AJ: IL-1 beta induces COX2, MMP-1, -3 and -13, ADAMTS-4, IL-1 beta and IL-6 in human tendon cells, J Orthop Res 2003, 21:256-264

75. Beltrami-Moreira M, Vromman A, Sukhova GK, Folco EJ, Libby P: Redundancy of IL-1 Isoform Signaling and Its Implications for Arterial Remodeling, PLoS One 2016, 11:e0152474

76. Sagulenko V, Thygesen SJ, Sester DP, Idris A, Cridland JA, Vajjhala PR, Roberts TL, Schroder K, Vince JE, Hill JM, Silke J, Stacey KJ: AIM2 and NLRP3 inflammasomes activate both apoptotic and pyroptotic death pathways via ASC, Cell Death Differ 2013, 20:1149-1160

77. Dai J, Tian J, Hou J, Xing L, Liu S, Ma L, Yu H, Ren X, Dong N, Yu B: Association between cholesterol crystals and culprit lesion vulnerability in patients with acute coronary syndrome: An optical coherence tomography study, Atherosclerosis 2016, 247:111-117

Figure legends

Figure 1. Electron micrographs of an external carotid artery intima containing foam cells, extracellular lipoprotein particles, and cholesterol crystals. **A, B:** TEM-micrograph representative of TEM-micrographic analysis of three plaques shows extracellular lipoprotein particles (black arrows in **B**) and intracellular lipid droplets. **B:** An enlargement of the boxed area in **A**. Based on TEM analysis, one plaque was selected for block face-scanning electron microscopy (SB-EM). **C:** The lowest block face image of the SB-EM dataset. **D:** 3D-model of extracellular lipid droplets, cholesterol crystals, and foam cells generated from SB-EM images. Cholesterol crystals (yellow) seem to grow out from large lipid droplets (short black arrowheads and inset). Large sheet-like crystals (black arrows) can be two-dimensionally as large as foam cells. The plasma membranes of the foam cells are artificially colored in transparent blue or green, the nuclei in light blue, and the intracellular lipid droplets in vermilion or maroon. Two cholesterol crystals are surrounded by the right-hand foam cell (white arrow). **E, F:** 3D models generated from tomographic reconstruction of the plaque used for SB-EM depict extracellular lipoprotein particles in a process of fusion. The scale bars indicate 5 μm (**A, C, D**), 0.5 μm (**B**), and 0.1 μm (**E, F**). Foam cells in **A**, **B**, **C**, and **D** are marked with asterisks.

Figure 2. Characterization of the extracellular lipoprotein particles. **A:** Binding of four different monoclonal antibodies generated against malonaldehyde-LDL or malondialdehyde-acetaldehyde-LDL to a single extracellular lipoprotein particle preparation. Fish gelatin was used as a negative control. The results are expressed as relative light units measured in 100 ms (RLU/100 ms). **B:** Circular dichroism analysis of LDL and extracellular lipoprotein particles. Representative spectrum of extracellular lipoprotein particles isolated from a pool of 10 pieces derived 10 individual plaques. Similar results were obtained with another preparation of extracellular lipoprotein particles prepared from a pool of 10 plaque pieces

derived from another 10 individual plaques. The samples were diluted to give a protein concentration of 50 μg/mL, and far-UV circular dichroism spectra were recorded using a 0.1 cm quartz cuvette in the region of 190 to 250 nm. Solid line, LDL; dashed line, extracellular lipoproteins; dotted line, zero level in CD[mdeg]. **C:** The presence of cholesterol crystals in the extracellular lipoprotein particle preparations was analyzed under polarized light. **D:** Lipid contents of the LDL and extracellular lipoprotein particles were determined by thin layer chromatography and are shown as mass percentages of the total mass (lipids + protein). Average of three preparations are shown. PC=phosphatidylcholine, SM=sphingomyelin, LPC=lysophosphatidylcholine, CE=cholesteryl ester, UC=unesterified cholesterol, FA=fatty acid, TAG=triacylglycerol.

Figure 3. Size and fractionation of extracellular lipoproteins. **A:** Sizes of LDL, VLDL, and extracellular lipoprotein particles were measured with dynamic light scattering. The data are representative of three individual preparations. The extracellular lipoproteins were fractionated based on particle size using rate zonal ultracentrifugation and the amounts of total cholesterol and triglycerides (**B**), and the amounts of apoB-100, apoA-I, and apoE in each fraction were determined (**C**). Three lipoprotein particle preparations, each from a pool of 10 to 20 pieces of individual plaques, were analyzed by rate zonal ultracentrifugation. The cholesterol and apoB-100 contents were analyzed in each of these preparations. Triglycerides, apoA-I, and apoE were analyzed from one preparation of 10 pooled plaques.

Figure 4. Inflammasome activation in human monocyte–derived macrophages. **A:** Monocyte-derived macrophages were primed with or without LPS for 4 h, after which extracellular lipoprotein particles or *in vitro*–generated cholesterol crystals were incubated with the cells for 18 h. The concentration of IL-1β was measured in cell culture supernatants (n = 6). **B:** LDL was modified by oxidation, proteolysis, or phospholipolysis either alone or in combination with LAL-induced cholesteryl ester hydrolysis for 18 h. Native or modified

LDL (n = 6–12) was then incubated with LPS-primed or non-primed human monocyte–derived macrophages for 18 h after which the concentration of IL-1β was determined in the supernatants. **C:** LPS-primed human monocyte–derived macrophages were incubated with VLDL or VLDL modified with PLA_2 and LAL (n = 6–18) for 18 hours. After the incubation the concentrations of IL-1β were determined from the supernatants. **D:** LPS-primed human monocyte–derived macrophages were incubated with LDL, LDL modified with PLA_2 and LAL, or with extracellular lipoprotein particles in the absence or presence of caspase-1 inhibitor Z-YVAD or cytochalasin D (CD), an inhibitor of cytoskeletal movements (n=10 to 12). *P < 0.05; **P < 0.005. Each data point is shown as a diamond and averages are shown as columns. CC = Cholesterol crystal, LP = Extracellular lipoprotein particles, Ox-LDL = Cu-oxidized LDL, a-CT = α-chymotrypsin –modified LDL, SMase = sphingomyelinase-modified LDL, PLA_2 = phospholipase A_2-modified LDL, LAL = lysosomal acid lipase-modified LDL

Figure 5. Lipid accumulation in human monocyte–derived macrophages. LDL, VLDL, enzymatically modified LDL (LDL+PLA_2+LAL), enzymatically modified VLDL (VLDL+PLA_2+LAL), *in vitro*–generated cholesterol crystals (CC), and extracellular lipoproteins (LP) were applied to human primary monocyte–derived macrophages. After incubation for 18 h, the cellular lipid contents were analyzed by TLC (n = 3–9). *P < 0.05.CE = cholesteryl ester, TAG = triacylglycerol, UC = unesterified cholesterol. Averages of the individual data points are shown as columns.

Figure 6. Proposed role of extracellular lipoprotein particles in atherogenesis. Extracellular lipoprotein particles are derived from plasma apoB-containing lipoproteins by modification and aggregation. Such modifications can also induce formation of cholesterol crystals. The extracellular lipoprotein particles together with cholesterol crystals induce extracellular lipid

accumulation and can be taken up by macrophages, in which, together with cholesterol crystals, they induce foam cell formation and inflammasome activation with ensuing IL-1β secretion.

Figure 1

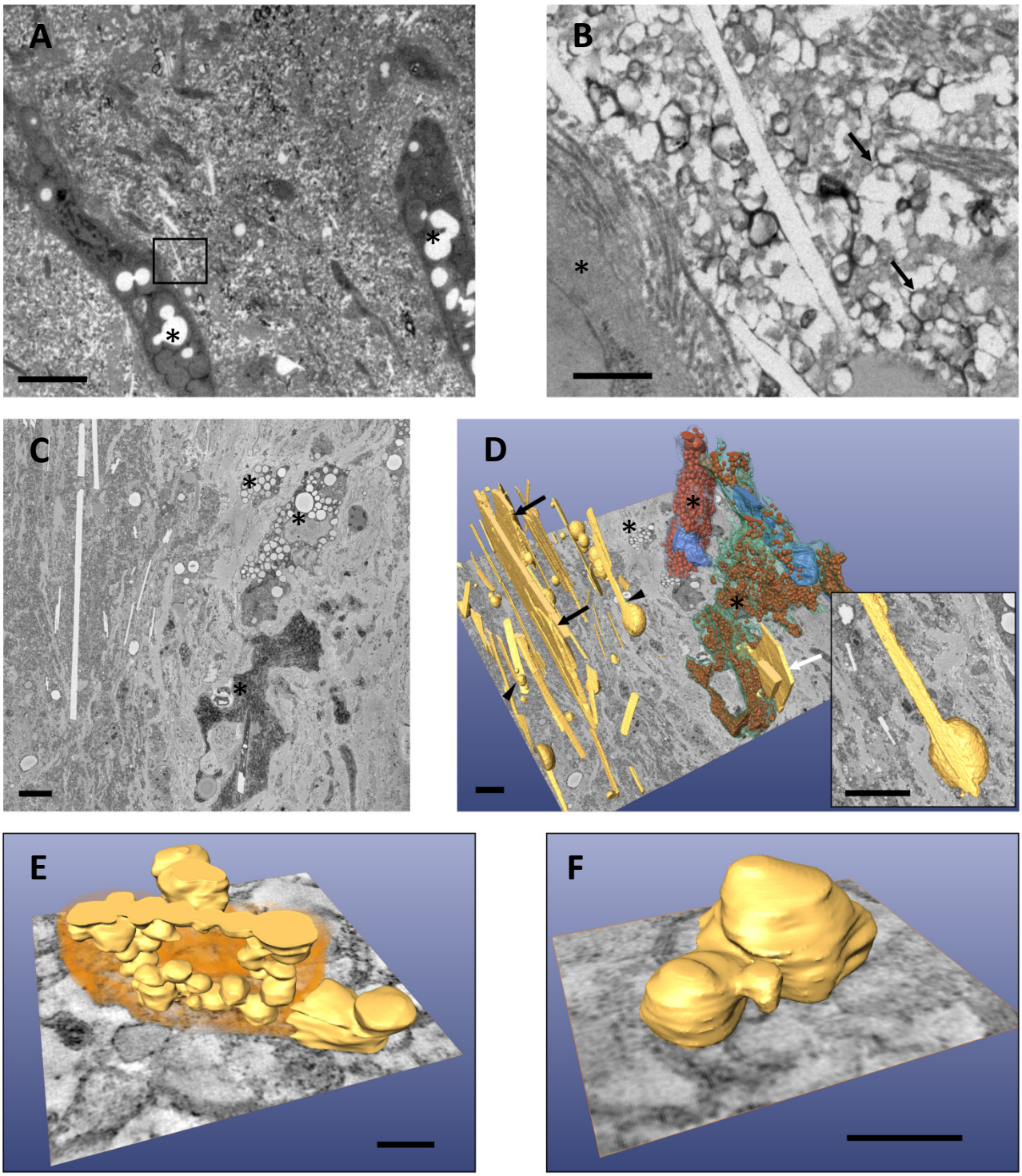

Figure 2

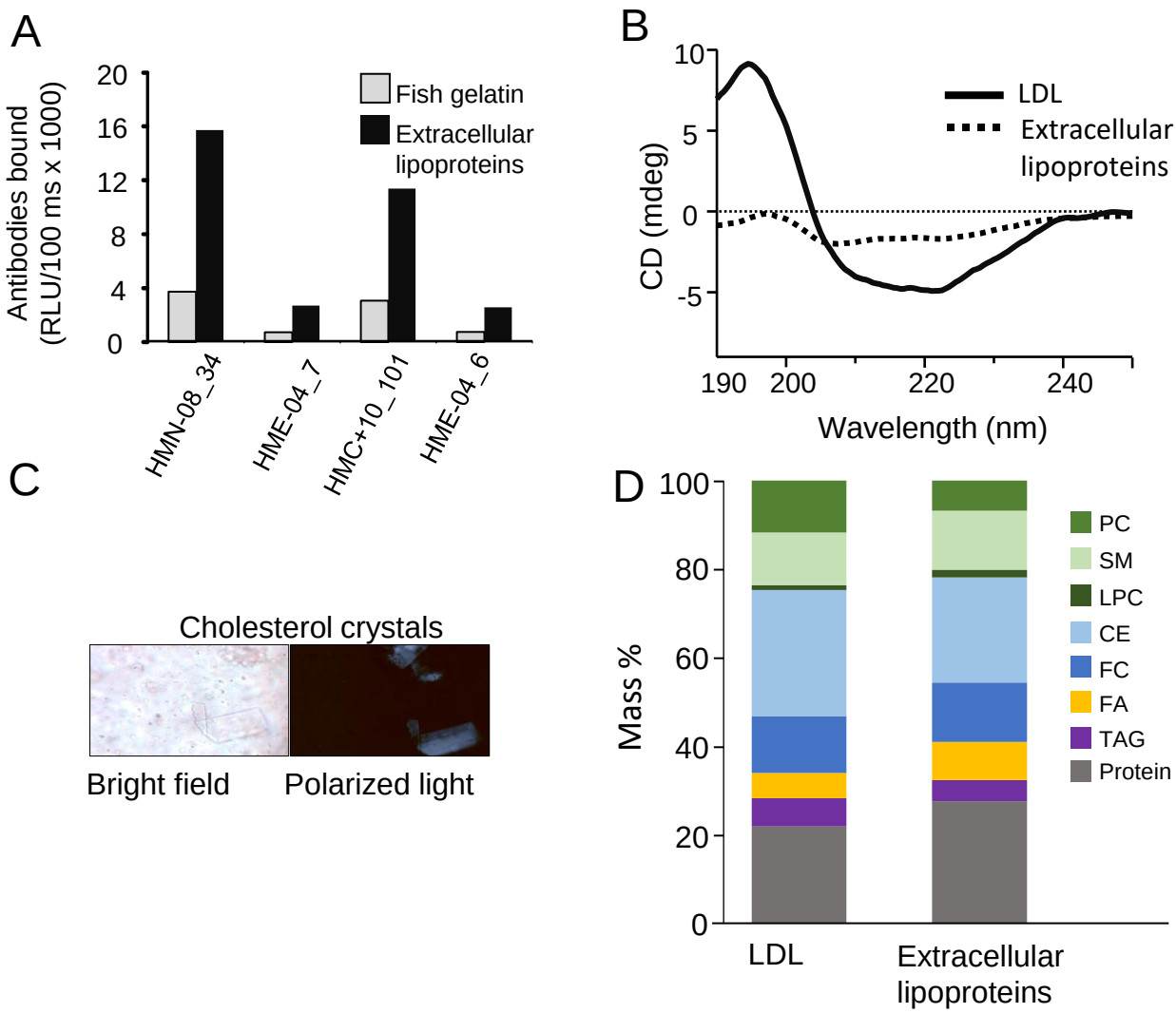
A
Antibodies bound (RLU/100 ms x 1000)
20
16
12
8
4
0
Fish gelatin
Extracellular lipoproteins
HMN-08_34
HME-04_7
HMC+10_101
HME-04_6
B
10
5
0
-5
CD (mdeg)
LDL
Extracellular lipoproteins
190
200
220
240
Wavelength (nm)
C
Cholesterol crystals
Bright field
Polarized light
D
100
80
60
40
20
0
Mass %
PC
SM
LPC
CE
FC
FA
TAG
Protein
LDL
Extracellular lipoproteins

Figure 3

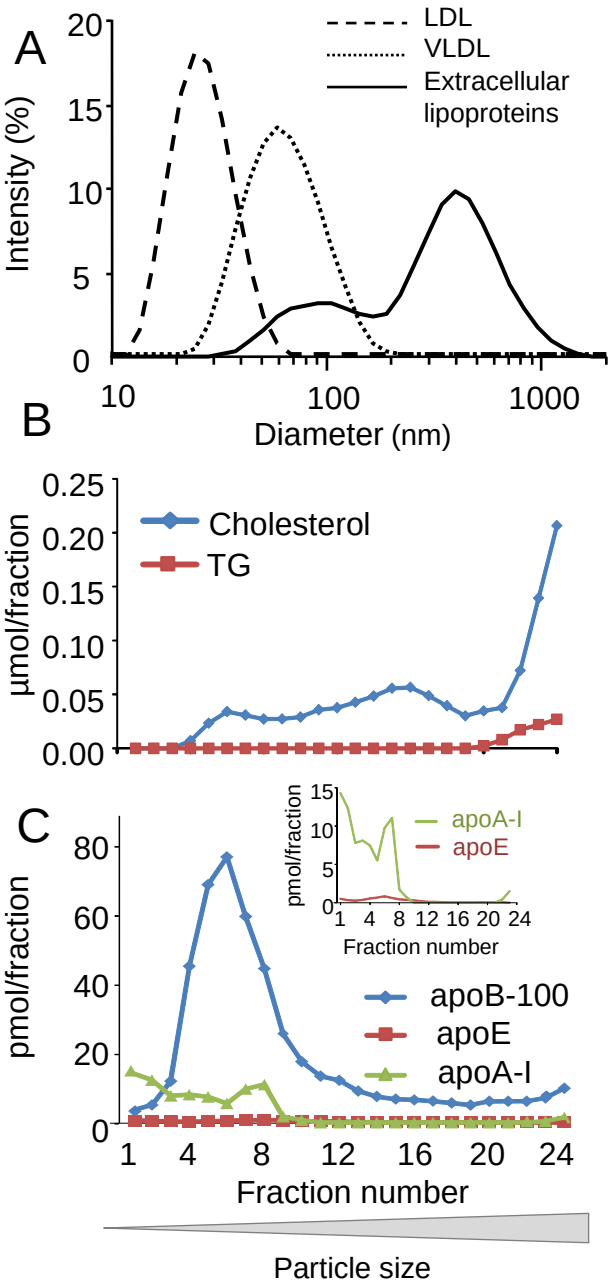
A
LDL
VLDL
Extracellular lipoproteins
Intensity (%)
20
15
10
5
0
10
100
1000
Diameter (nm)
B
µmol/fraction
0.25
0.20
0.15
0.10
0.05
0.00
Cholesterol
TG
C
pmol/fraction
80
60
40
20
0
1 4 8 12 16 20 24
Fraction number
apoB-100
apoE
apoA-I
pmol/fraction
15
10
5
0
1 4 8 12 16 20 24
Fraction number
apoA-I
apoE
Particle size

Figure 4

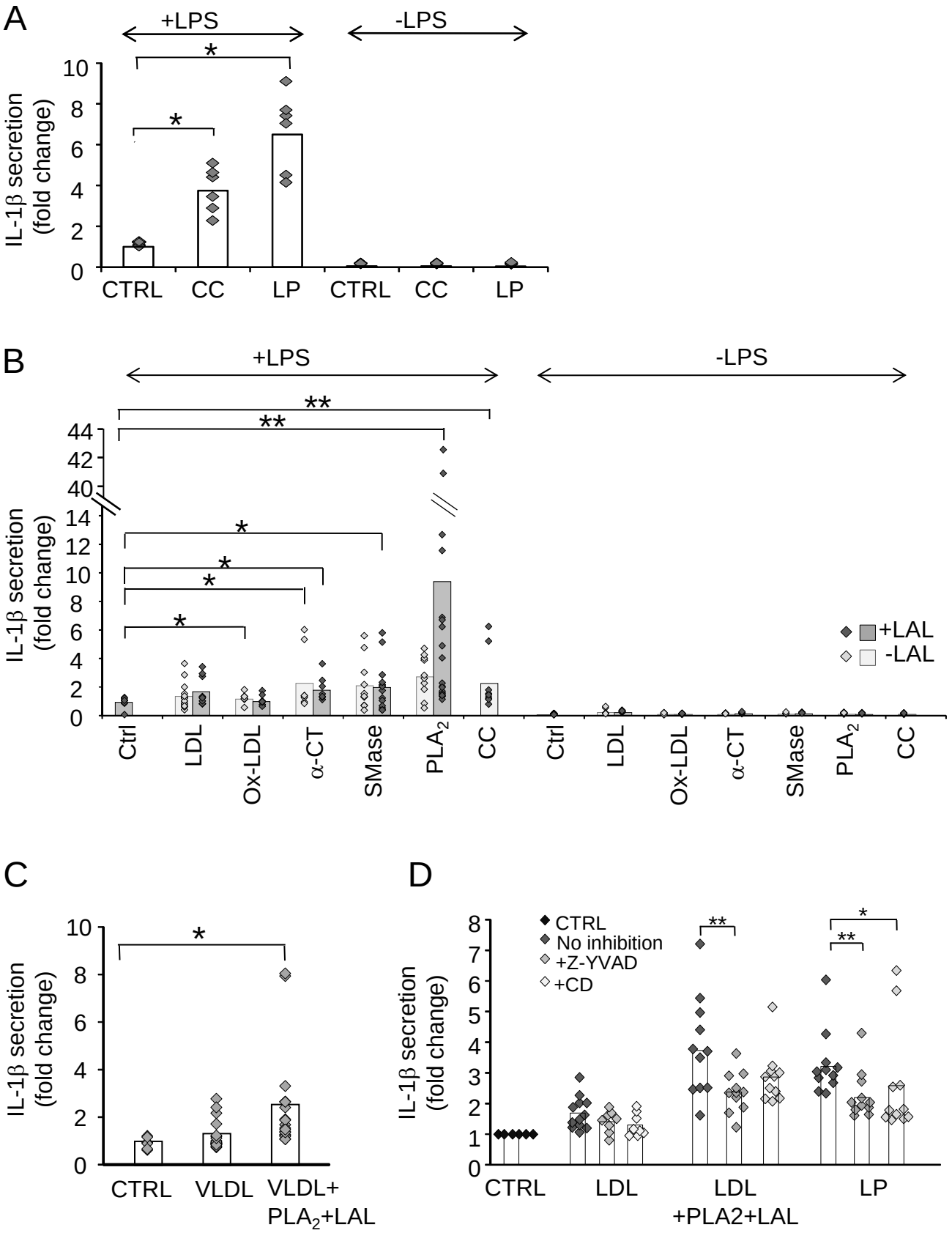
A
+LPS
-LPS
IL-1β secretion (fold change)
CTRL
CC
LP
B
+LPS
-LPS
IL-1β secretion (fold change)
+LAL
-LAL
Ctrl
LDL
Ox-LDL
α-CT
SMase
PLA2
CC
C
IL-1β secretion (fold change)
CTRL
VLDL
VLDL+ PLA2+LAL
D
IL-1β secretion (fold change)
CTRL
No inhibition
+Z-YVAD
+CD
CTRL
LDL
LDL +PLA2+LAL
LP

Figure 5

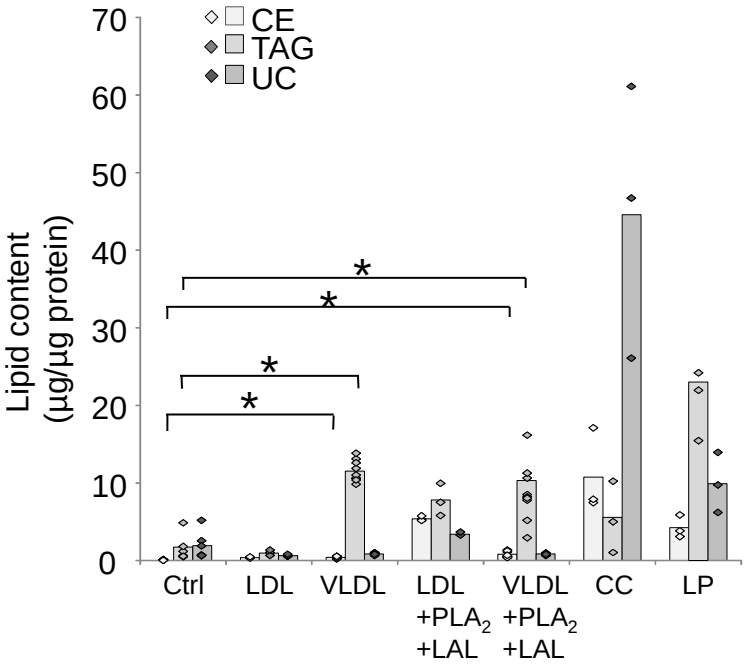
CE
TAG
UC
Lipid content (µg/µg protein)
70
60
50
40
30
20
10
0
*
*
*
*
Ctrl
LDL
VLDL
LDL +PLA2 +LAL
VLDL +PLA2 +LAL
CC
LP

Figure 6

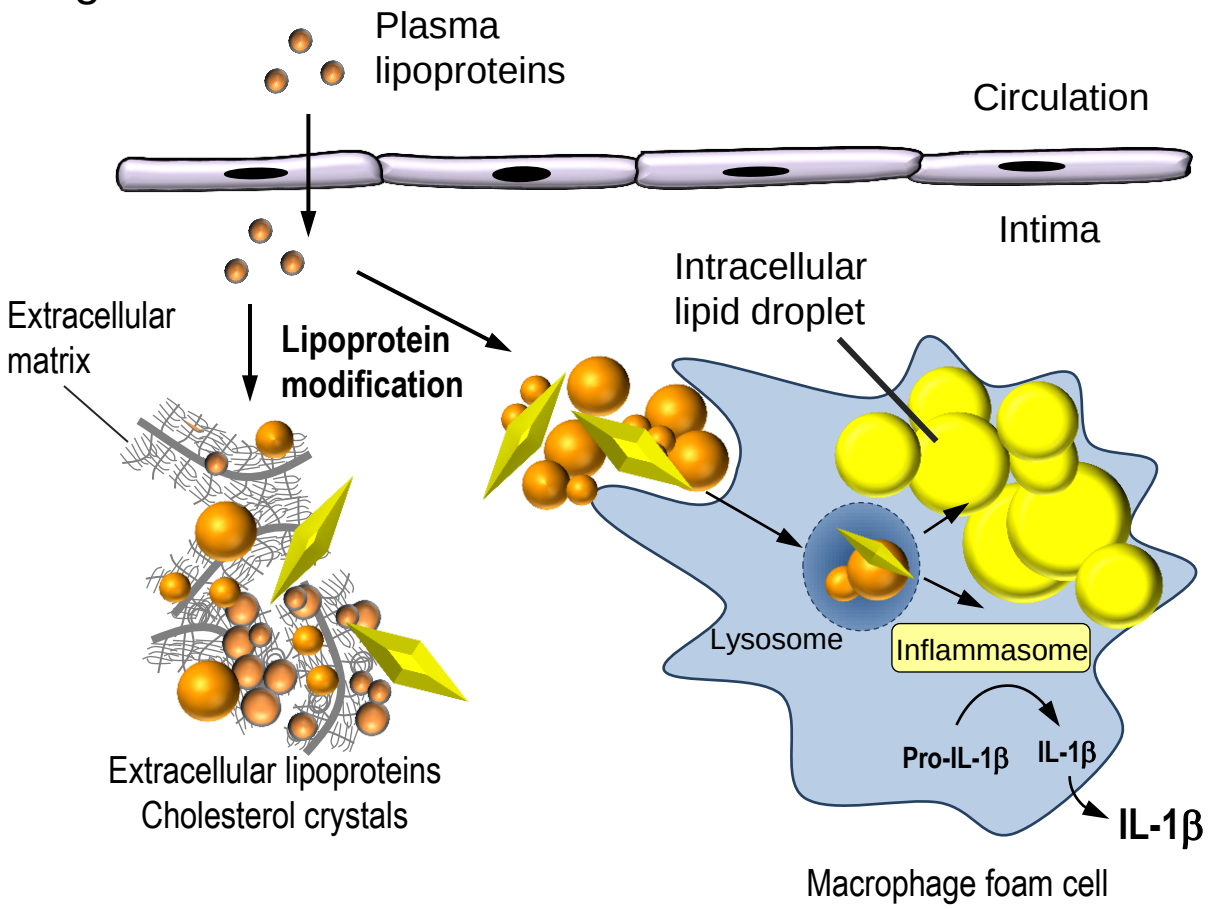
Plasma
lipoproteins
Circulation
Intima
Intracellular
lipid droplet
Extracellular
matrix
Lipoprotein
modification
Lysosome
Inflammasome
Pro-IL-1β
IL-1β
IL-1β
Extracellular lipoproteins
Cholesterol crystals
Macrophage foam cell

SUPPLEMENTAL MATERIAL

Supplemental Figure legends

Supplemental Figure 1. Electron micrograph of a partial cross section of a common carotid artery. (A) Combined TEM micrographs show a 420 μm partial cross section of a common carotid artery. The lumen and endothelial surface appear at the bottom of the image. Above the endothelium, foam cells are seen, and above the layer of foam cells, large cholesterol crystals are present. Panels B–E show enlargements of the boxed areas. (B) Large cholesterol crystals form massive clusters. (C, D) Small cholesterol crystals are found both inside and outside of the foam cells (circles in panel D) (E, F) Small cholesterol crystals among the extracellular lipoprotein particles (circles in panel F). Scale bars and magnification factors: A 20 μm, 200x; B, 5 μm, 1000x; C, 20 μm, 400x; D, 2 μm, 2500x; E, 5 μm, 1000x; F, 2 μm, 4000x.

Supplemental Figure 2. Induction of cholesterol crystal formation via modification of LDL. LDL was modified by oxidation, proteolysis, or lipolysis to induce perturbations in the surface of the particles, after which the pre-modified particles were treated with lysosomal acid lipase (LAL) to induce cholesteryl ester hydrolysis. The samples were analyzed for the presence of cholesterol crystals by birefringence under polarized light. (A) LDL oxidized with $CuSO_4$ and lipolyzed with LAL. (B) LDL modified with phospholipase A_2 (PLA_2) and LAL. (C) LDL modified with sphingomyelinase (SMase) and LAL. (D) LDL proteolyzed first with α-chymotrypsin (αCT) and then treated with LAL. (E) LDL lipolyzed with LAL. Scale bar 10 μm (A–E).

Supplemental Figure 3. Representative immunohistochemical stainings of apolipoproteins in human carotid atherosclerotic intima. The areas with black borders in Panels A–I are shown enlarged in panels B–J, respectively. (A, B) Polyclonal anti-apoB-100 antibody; (C, D) monoclonal anti-apoB-100 antibody (E, F); monoclonal anti-ApoE antibody; (G, H) monoclonal anti-ApoA-I antibody, and (I, J) monoclonal anti-ApoC-III antibody. Scale bars 200 μm (A, C, E, G, I) or 100 μm (B, D, F, H, J).

Supplemental Figure 4. Analysis of apoB-100 and apoE contents of the particles. (A) Extracellular lipoprotein particles were isolated from human carotid arteries and then analyzed for the presence of apoB-100 using a chemiluminescent assay. The results are expressed as relative light units measured in 100 ms (RLU/100 ms). (B) The isolated extracellular lipoprotein particles (total protein concentration 0.8 mg/ml and 0.3 mg/ml in samples #1 and #2, respectively), VLDL, and LDL particles were analyzed by Western blot using a polyclonal anti-apoB-100 antibody and a polyclonal anti-apoE antibody. (C) Extracellular lipoprotein particles and homogenized solid tissue remnants were analyzed by Western blot using polyclonal anti-Plin1 antibody. Lanes: 1, size standards; 2-4, solid fragments of three different isolations; 5. Isolated extracellular lipoproteins from a single isolation. Each isolation round contains tissue from 10–20 different carotid arteries. LP= Extracellular lipoprotein particles

Supplemental Figure 5. Mass spectrometric analysis of choline phospholipids in isolated extracellular lipoprotein particles and in LDL. Lipid species profiles of the extracellular lipoprotein particles from (n= 4 pooled isolations, each pool containing extracellular lipoprotein particles from 10–20 plaques) and LDL (n=3) were analyzed with ESI-mass spectrometry as described in Methods. Each column represents a molar percentage of the lipid species indicated.

Supplemental Figure 6. Mass spectrometric analysis of cholesteryl esters in isolated extracellular lipoprotein particles and in LDL. Analysis of cholesteryl ester species of extracellular lipoprotein particles from (n= 4 pooled isolations, each pool containing extracellular lipoprotein particles from 10–20 plaques) and LDL (n=3) by their fatty acid composition was performed by ESI-mass spectrometry, as described in the

Methods. Each column represents a molar percentage of an individual cholesteryl ester species from the sum of all cholesteryl ester species.

Supplemental Figure 1

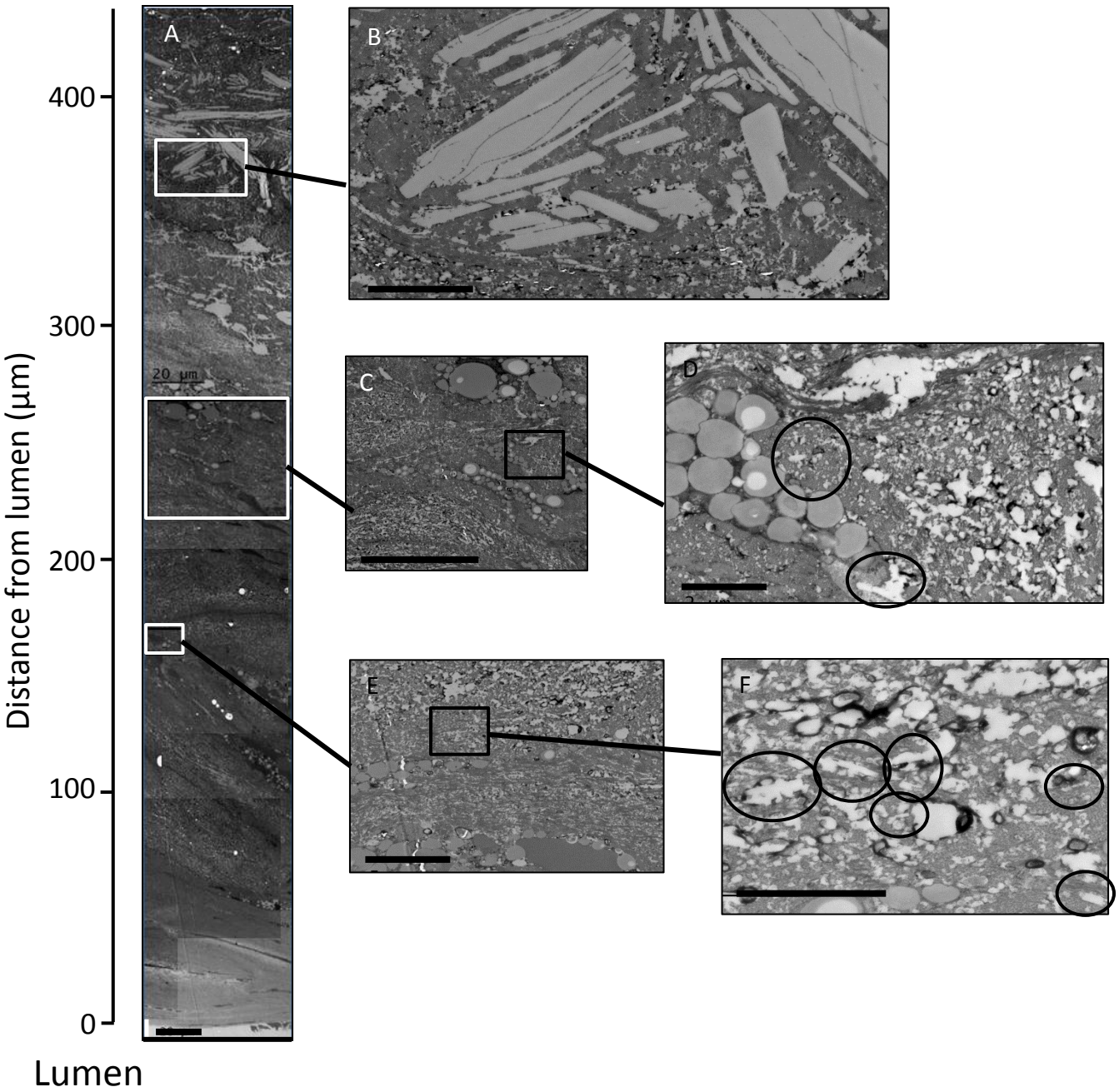

Supplemental Figure 2

LDL+oxidation+LAL

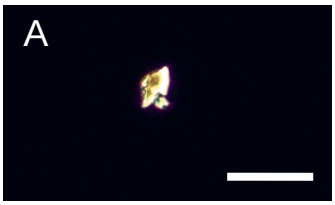

LDL+PLA_2 +LAL

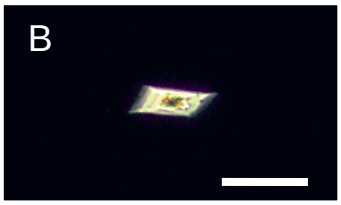

LDL+SMase+LAL

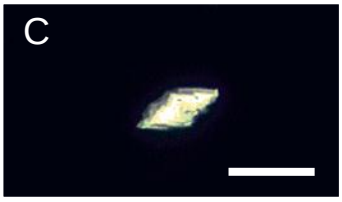

LDL+α-CT+LAL

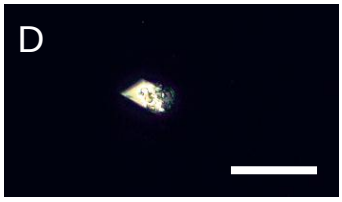

LDL+LAL

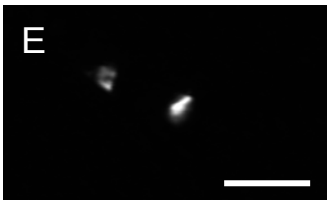

Supplemental Figure 3

Anti-apoB, polyclonal

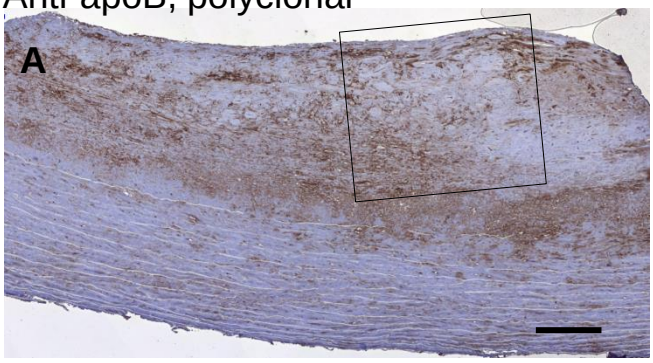

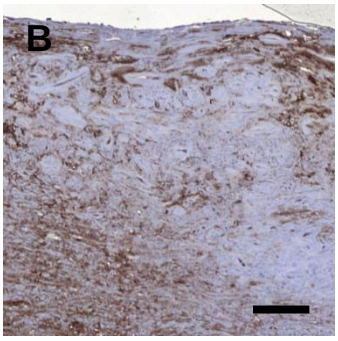

Anti-apoB, monoclonal

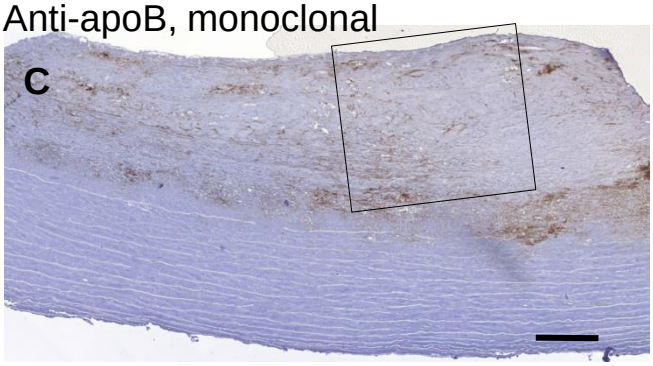

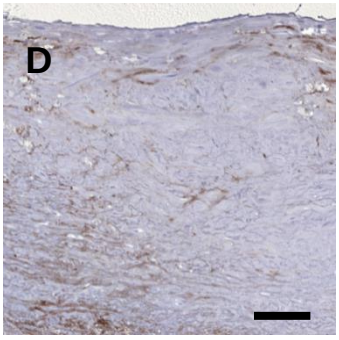

Anti-apoE

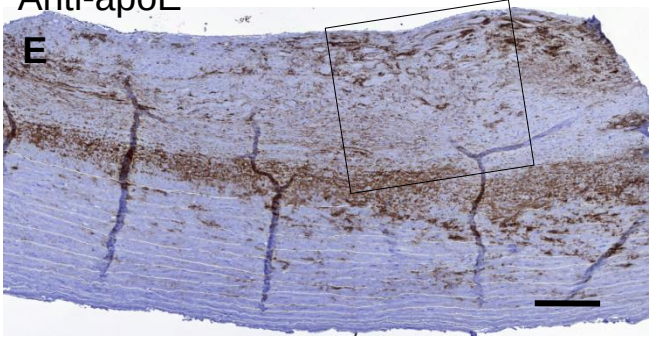

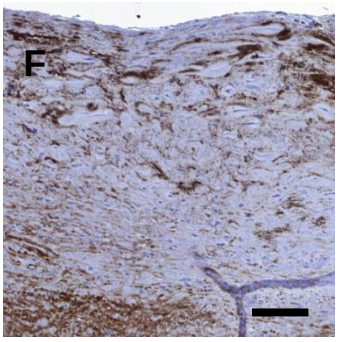

Anti-apoA-1

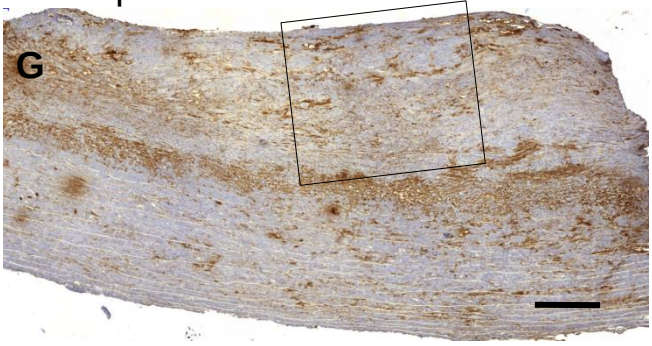

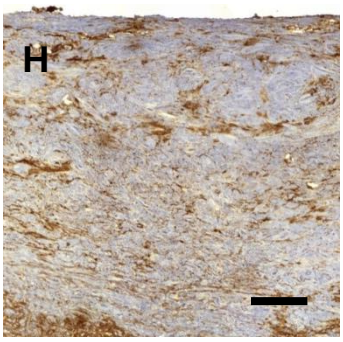

Anti-apoC-III

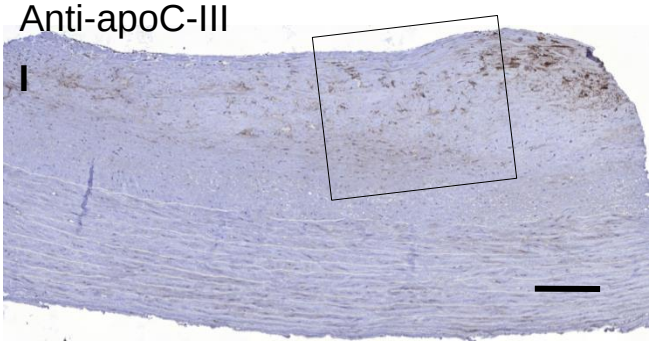

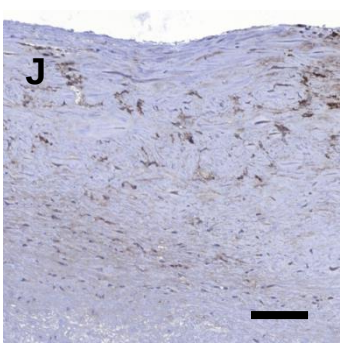

Supplemental Figure 4

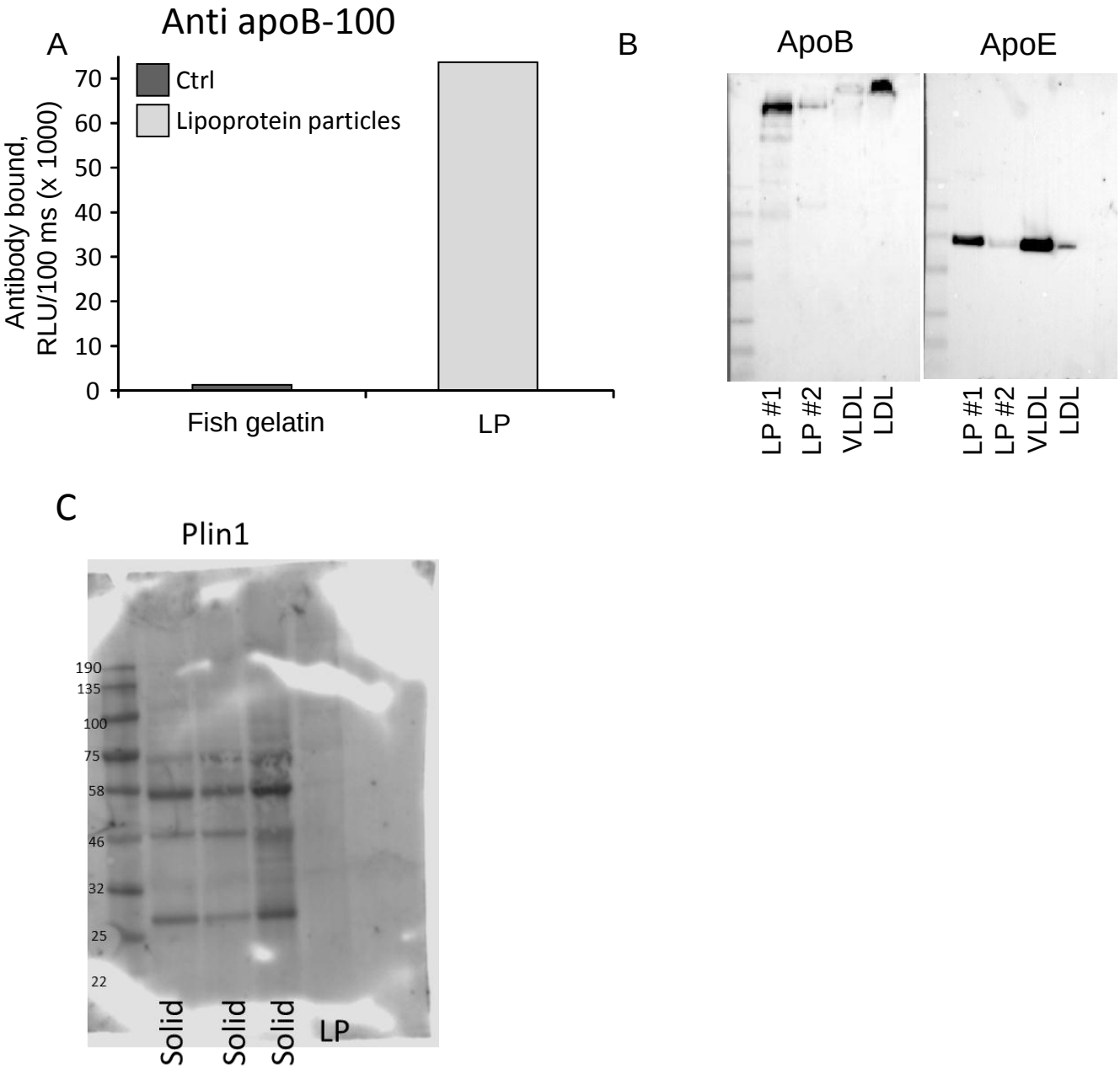

Supplemental Figure 5

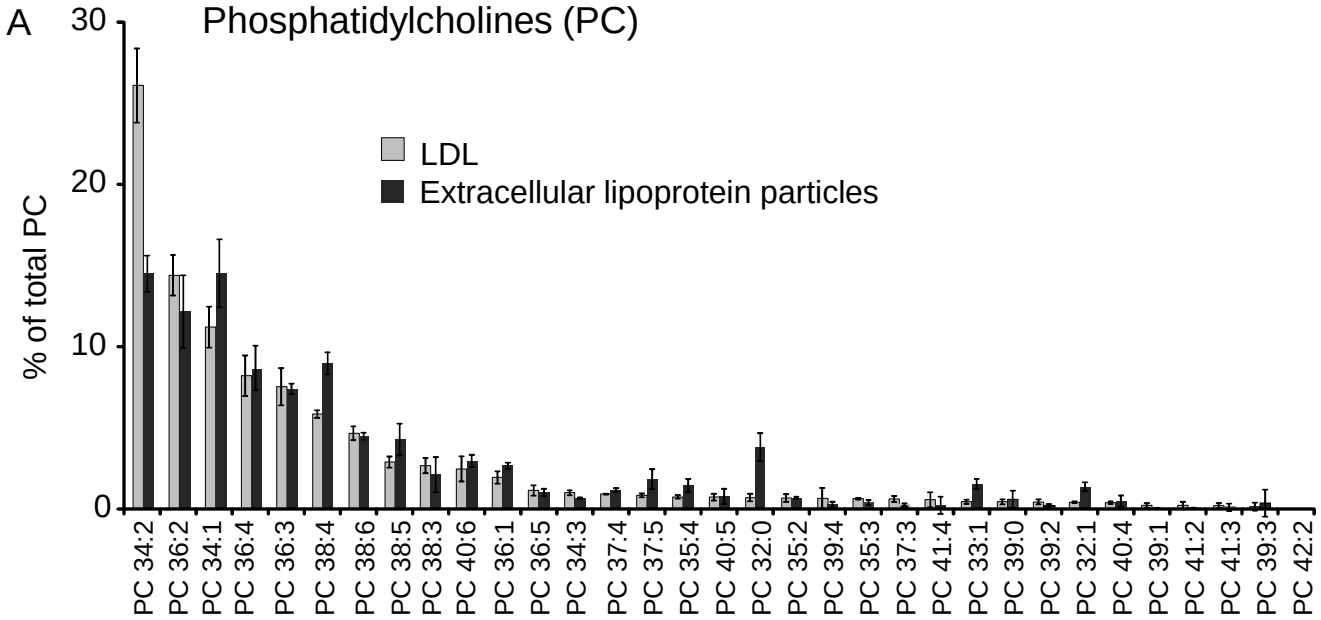

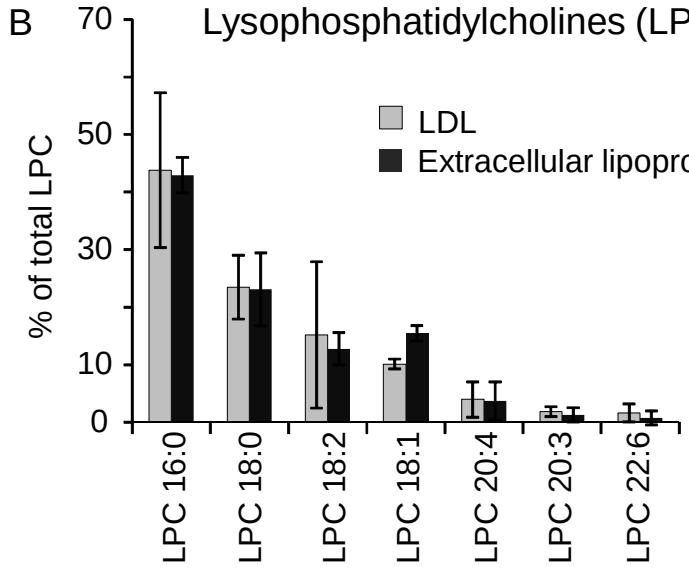

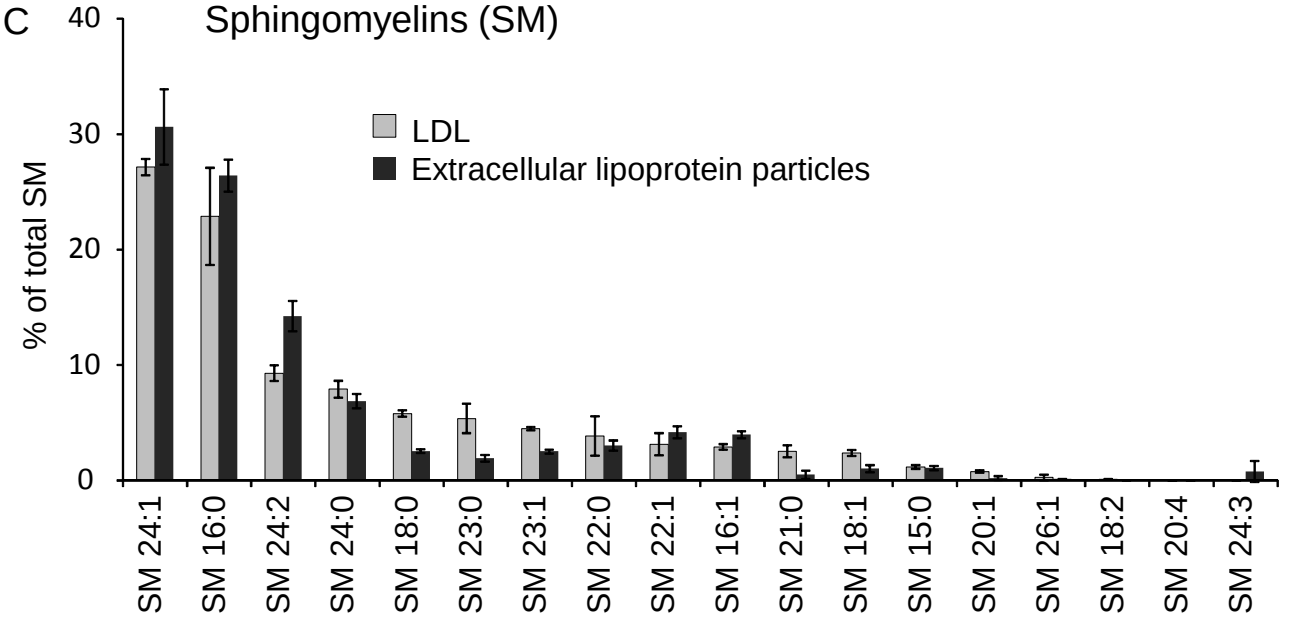

Supplemental Figure 6

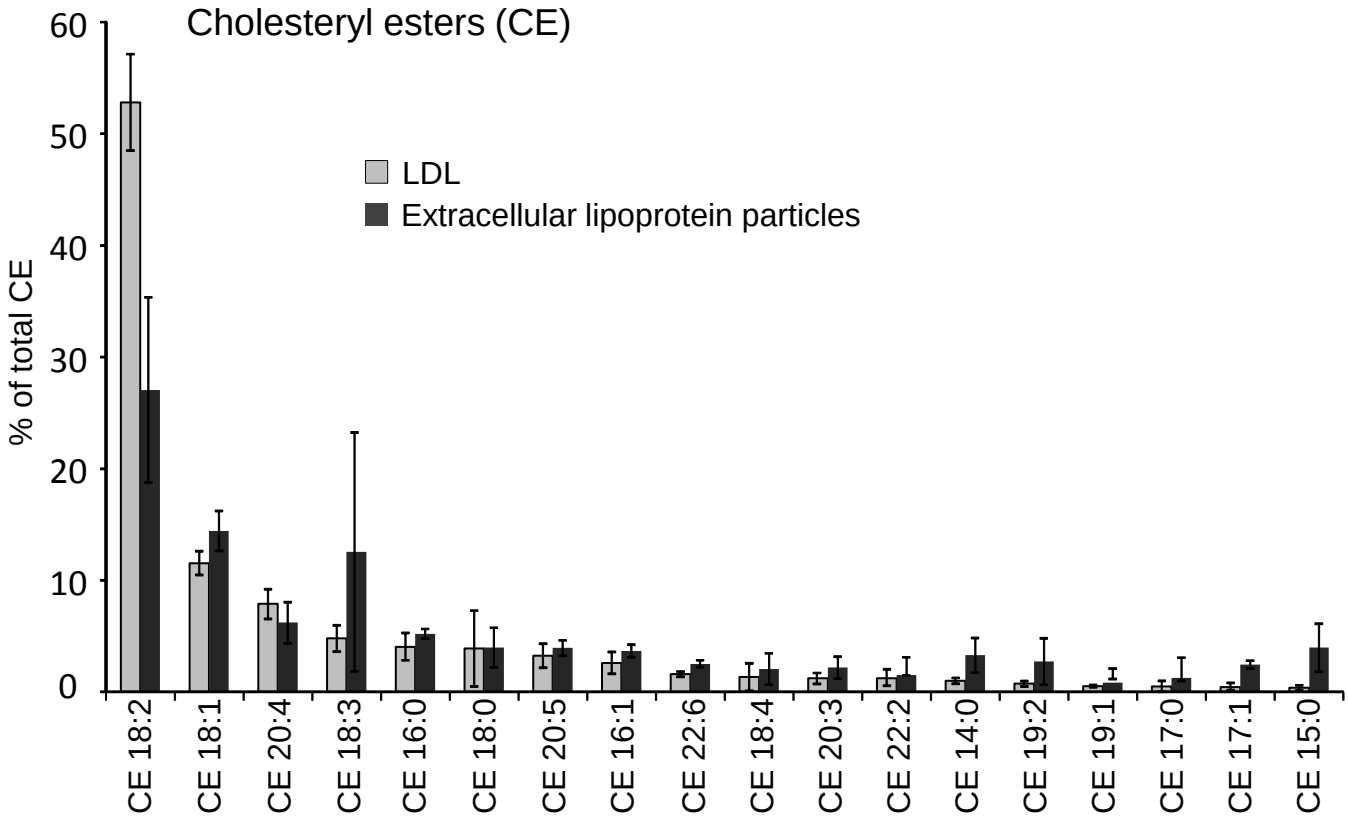

Supplemental Table legend:

Supplemental Table 1. Protein mass spectrometry on the extracellular lipoprotein particles. Criteria to include proteins: protein sequence covered at least 10 %, 5 or more peptides recognized, isoforms with identical mass removed, and only proteins with GREEN auto curate were accepted. Proteins were ordered according to protein top3 Matched Peptide Intensity Sum.

Supplemental Video legends:

Supplemental video 1. Serial block faces (340 layers at 40 nm intervals) imaged generated from a carotid artery intima.

Supplemental video 2. 3-D model of a carotid artery intima generated from a SB-EM dataset comprising 340 block face images at 40 nm intervals. Two foam cells (plasma membranes) are modeled in transparent green and light blue, their nuclei in blue, and their cytoplasmic lipid droplets in vermilion and maroon. Cholesterol crystals and extracellular particles are shown in yellow.

Supplemental video 3. Extracellular particles in a process of fusion modeled from a TEM tomogram of a carotid artery intima. The extracellular particles are modeled in yellow. Multilamellar phospholipid surface is modeled in dark yellow.

Supplemental Table 1. Protein mass spectrometry on the extracellular lipoprotein particles. Criteria to include proteins: protein sequence covered at least 10 %, 5 or more peptides recognized, isoforms with identical mass removed, and only proteins with GREEN auto curate were accepted. Proteins were ordered according to protein top3 Matched Peptide Intensity Sum. The lipoporoteins found are marked with bold textype.

	Protein Entry	Protein Accession (Swiss Prot)	Protein Description	Protein score	Protein average Mass	Protein matched Peptides	Protein sequence Coverage (%)	Protein top3 Matched Peptide Intensity Sum	Protein Auto Curate
1	**APOA1_HUMAN**	**P02647**	**Apolipoprotein A-I OS=Homo sapiens GN=APOA1 PE=1 SV=1**	**75923**	**30778**	**25**	**59,9**	**22155870**	**Green**
2	HBB_HUMAN	P68871	Hemoglobin subunit beta OS=Homo sapiens GN=HBB PE=1 SV=2	96003	16112	10	76,9	19712860	Green
3	ACTH_HUMAN	P63267	Actin_ gamma-enteric smooth muscle OS=Homo sapiens GN=ACTG2 PE=1 SV=1	41893	42276	25	55,1	11708810	Green
4	HBA_HUMAN	P69905	Hemoglobin subunit alpha OS=Homo sapiens GN=HBA1 PE=1 SV=2	9476	15315	7	57,8	8356400	Green
5	ACTB_HUMAN	P60709	Actin_ cytoplasmic 1 OS=Homo sapiens GN=ACTB PE=1 SV=1	25631	42079	25	58,7	8111540	Green
6	**APOB_HUMAN**	**P04114**	**Apolipoprotein B-100 OS=Homo sapiens GN=APOB PE=1 SV=2**	**22426**	**516974**	**245**	**49,3**	**7613403**	**Green**
7	**APOE_HUMAN**	**P02649**	**Apolipoprotein E OS=Homo sapiens GN=APOE PE=1 SV=1**	**33076**	**36268**	**28**	**62,8**	**7285466**	**Green**
8	**APOD_HUMAN**	**P05090**	**Apolipoprotein D OS=Homo sapiens GN=APOD PE=1 SV=1**	**8808**	**21561**	**6**	**24,9**	**4833133**	**Green**
9	IGHG1_HUMAN	P01857	Ig gamma-1 chain C region OS=Homo sapiens GN=IGHG1 PE=1 SV=1	12182	36619	12	42,7	4587963	Green
10	TAGL_HUMAN	Q01995	Transgelin OS=Homo sapiens GN=TAGLN PE=1 SV=4	11417	22668	13	53,7	2257899	Green
11	MYL6_HUMAN	P60660	Myosin light polypeptide 6 OS=Homo sapiens GN=MYL6 PE=1 SV=2	24147	17101	14	72,2	2254040	Green
12	**APOC3_HUMAN**	**P02656**	**Apolipoprotein C-III OS=Homo sapiens GN=APOC3 PE=1 SV=1**	**22119**	**10852**	**5**	**53,5**	**2111973**	**Green**
13	MYH11_HUMAN	P35749	Myosin-11 OS=Homo sapiens GN=MYH11 PE=1 SV=3	11022	228195	73	40,0	2101943	Green
14	VIME_HUMAN	P08670	Vimentin OS=Homo sapiens GN=VIM PE=1 SV=4	7384	53709	25	47,2	1957304	Green

15	MYH9_HUMAN	P35579	Myosin-9 OS=Homo sapiens GN=MYH9 PE=1 SV=4	10865	227787	73	38,8	1762550	Green
16	MYL9_HUMAN	P24844	Myosin regulatory light polypeptide 9 OS=Homo sapiens GN=MYL9 PE=1 SV=4	34644	19884	18	72,7	1475450	Green
17	A1AT_HUMAN	P01009	Alpha-1-antitrypsin OS=Homo sapiens GN=SERPINA1 PE=1 SV=3	11233	46908	17	46,4	1390492	Green
18	IGHG2_HUMAN	P01859	Ig gamma-2 chain C region OS=Homo sapiens GN=IGHG2 PE=1 SV=2	3789	36528	6	19,0	1366743	Green
19	MYH10_HUMAN	P35580	Myosin-10 OS=Homo sapiens GN=MYH10 PE=1 SV=3	5865	229969	73	42,2	1334933	Green
20	VTNC_HUMAN	P04004	Vitronectin OS=Homo sapiens GN=VTN PE=1 SV=1	4901	55104	11	33,1	1275587	Green
21	POTEE_HUMAN	Q6S8J3	POTE ankyrin domain family member E OS=Homo sapiens GN=POTEE PE=1 SV=3	11939	122936	19	23,3	1245045	Green
22	CLUS_HUMAN	P10909	Clusterin OS=Homo sapiens GN=CLU PE=1 SV=1	8346	53065	12	24,9	1173977	Green
23	ACTBM_HUMAN	Q9BYX7	Putative beta-actin-like protein 3 OS=Homo sapiens GN=POTEKP PE=5 SV=1	11040	42359	6	20,5	1156171	Green
24	TPM2_HUMAN	P07951-2	Isoform 2 of Tropomyosin beta chain OS=Homo sapiens GN=TPM2	5643	33047	9	30,6	928862	Green
25	K2C1_HUMAN	P04264	Keratin_ type II cytoskeletal 1 OS=Homo sapiens GN=KRT1 PE=1 SV=6	4495	66210	21	31,2	925092	Green
26	MFGM_HUMAN	Q08431-2	Isoform 2 of Lactadherin OS=Homo sapiens GN=MFGE8	7472	35474	12	43,0	917399	Green
27	IGHA1_HUMAN	P01876	Ig alpha-1 chain C region OS=Homo sapiens GN=IGHA1 PE=1 SV=2	3404	38510	5	16,4	901777	Green
28	LAC2_HUMAN	P0CG05	Ig lambda-2 chain C regions OS=Homo sapiens GN=IGLC2 PE=1 SV=1	26144	11465	5	62,3	831052	Green
29	GELS_HUMAN	P06396-2	Isoform 2 of Gelsolin OS=Homo sapiens GN=GSN	3908	80926	13	26,4	823551	Green
30	TRFE_HUMAN	P02787	Serotransferrin OS=Homo sapiens GN=TF PE=1 SV=3	2422	79345	18	26,7	742905	Green
31	RAB1A_HUMAN	P62820	Ras-related protein Rab-1A OS=Homo sapiens GN=RAB1A PE=1 SV=3	43052	22906	12	74,6	678850	Green
32	TPM4_HUMAN	P67936	Tropomyosin alpha-4 chain OS=Homo sapiens GN=TPM4 PE=1 SV=3	1813	28636	8	27,8	644756	Green
33	SAMP_HUMAN	P02743	Serum amyloid P-component OS=Homo sapiens GN=APCS PE=1 SV=2	6433	25501	9	29,6	640091	Green
34	A2MG_HUMAN	P01023	Alpha-2-macroglobulin OS=Homo sapiens GN=A2M PE=1 SV=3	1358	164717	19	19,5	491581	Green
35	TPM1_HUMAN	P09493	Tropomyosin alpha-1 chain OS=Homo sapiens GN=TPM1 PE=1 SV=2	1114	32766	7	16,6	490363	Green
36	TBB5_HUMAN	P07437	Tubulin beta chain OS=Homo sapiens GN=TUBB PE=1 SV=2	5096	50127	13	44,1	452320	Green
37	FLNA_HUMAN	P21333	Filamin-A OS=Homo sapiens GN=FLNA PE=1 SV=4	1329	283477	43	23,2	424363	Green

38	FIBG_HUMAN	P02679-2	Isoform Gamma-A of Fibrinogen gamma chain OS=Homo sapiens GN=FGG	7576	50124	12	26,8	422607	Green
39	HPT_HUMAN	P00738	Haptoglobin OS=Homo sapiens GN=HP PE=1 SV=1	690	45890	8	20,2	408679	Green
40	IGHM_HUMAN	P01871	Ig mu chain C region OS=Homo sapiens GN=IGHM PE=1 SV=3	3213	49991	10	24,1	401535	Green
41	RB11B_HUMAN	Q15907	Ras-related protein Rab-11B OS=Homo sapiens GN=RAB11B PE=1 SV=4	4656	24603	7	53,2	390997	Green
42	RAB7A_HUMAN	P51149	Ras-related protein Rab-7a OS=Homo sapiens GN=RAB7A PE=1 SV=1	4534	23775	7	42,5	357066	Green
43	CO3_HUMAN	P01024	Complement C3 OS=Homo sapiens GN=C3 PE=1 SV=2	1012	188688	32	19,6	342297	Green
44	ML12B_HUMAN	O14950	Myosin regulatory light chain 12B OS=Homo sapiens GN=MYL12B PE=1 SV=2	28306	19836	14	72,7	336412	Green
45	GNAI2_HUMAN	P04899	Guanine nucleotide-binding protein G(i) subunit alpha-2 OS=Homo sapiens GN=GNAI2 PE=1 SV=3	2058	41021	8	21,4	335244	Green
46	FIBB_HUMAN	P02675	Fibrinogen beta chain OS=Homo sapiens GN=FGB PE=1 SV=2	2571	56613	10	31,2	329146	Green
47	RL40_HUMAN	P62987	Ubiquitin-60S ribosomal protein L40 OS=Homo sapiens GN=UBA52 PE=1 SV=2	8111	15013	5	47,7	322508	Green
48	ANXA2_HUMAN	P07355	Annexin A2 OS=Homo sapiens GN=ANXA2 PE=1 SV=2	2001	38832	10	35,1	321505	Green
49	AXA2L_HUMAN	A6NMY6	Putative annexin A2-like protein OS=Homo sapiens GN=ANXA2P2 PE=5 SV=2	1887	38830	8	28,6	321505	Green
50	CAD13_HUMAN	P55290	Cadherin-13 OS=Homo sapiens GN=CDH13 PE=1 SV=1	3228	78743	13	22,3	310060	Green
51	CATD_HUMAN	P07339	Cathepsin D OS=Homo sapiens GN=CTSD PE=1 SV=1	1208	45066	9	20,9	306636	Green
52	RAB14_HUMAN	P61106	Ras-related protein Rab-14 OS=Homo sapiens GN=RAB14 PE=1 SV=4	2113	24125	7	34,4	296955	Green
53	G3P_HUMAN	P04406-2	Isoform 2 of Glyceraldehyde-3-phosphate dehydrogenase OS=Homo sapiens GN=GAPDH	3589	31719	7	32,1	293891	Green
54	RAB2A_HUMAN	P61019	Ras-related protein Rab-2A OS=Homo sapiens GN=RAB2A PE=1 SV=1	2006	23717	8	46,7	291363	Green
55	CAH1_HUMAN	P00915	Carbonic anhydrase 1 OS=Homo sapiens GN=CA1 PE=1 SV=2	1814	28927	5	29,1	279235	Green
56	FIBA_HUMAN	P02671	Fibrinogen alpha chain OS=Homo sapiens GN=FGA PE=1 SV=2	400	95715	15	11,0	278846	Green
57	HSPB1_HUMAN	P04792	Heat shock protein beta-1 OS=Homo sapiens GN=HSPB1 PE=1 SV=2	1596	22840	5	29,3	272562	Green
58	**APOA4_HUMAN**	**P06727**	**Apolipoprotein A-IV OS=Homo sapiens GN=APOA4 PE=1 SV=3**	**695**	**45399**	**8**	**22,7**	**267588**	**Green**
59	RB11A_HUMAN	P62491	Ras-related protein Rab-11A OS=Homo sapiens GN=RAB11A PE=1 SV=3	3158	24508	6	40,3	257958	Green

60	RAB1B_HUMAN	Q9H0U4	Ras-related protein Rab-1B OS=Homo sapiens GN=RAB1B PE=1 SV=1	40696	22342	9	61,7	256012	Green
61	FINC_HUMAN	P02751	Fibronectin OS=Homo sapiens GN=FN1 PE=1 SV=4	467	266218	29	11,1	255394	Green
62	HBD_HUMAN	P02042	Hemoglobin subunit delta OS=Homo sapiens GN=HBD PE=1 SV=2	37253	16170	6	49,0	254513	Green
63	ANXA1_HUMAN	P04083	Annexin A1 OS=Homo sapiens GN=ANXA1 PE=1 SV=2	3373	38942	13	45,7	252360	Green
64	RHG01_HUMAN	Q07960	Rho GTPase-activating protein 1 OS=Homo sapiens GN=ARHGAP1 PE=1 SV=1	2144	50493	7	25,5	245082	Green
65	ACTN1_HUMAN	P12814-2	Isoform 2 of Alpha-actinin-1 OS=Homo sapiens GN=ACTN1	836	103280	18	33,0	234403	Green
66	CO9_HUMAN	P02748	Complement component C9 OS=Homo sapiens GN=C9 PE=1 SV=2	370	64656	10	20,0	233880	Green
67	VINC_HUMAN	P18206-2	Isoform 1 of Vinculin OS=Homo sapiens GN=VCL	2374	117293	17	22,0	223471	Green
68	NIBAN_HUMAN	Q9BZQ8	Protein Niban OS=Homo sapiens GN=FAM129A PE=1 SV=1	644	104104	11	14,7	211735	Green
69	TBB3_HUMAN	Q13509	Tubulin beta-3 chain OS=Homo sapiens GN=TUBB3 PE=1 SV=2	4046	50889	14	40,9	210320	Green
70	PON1_HUMAN	P27169	Serum paraoxonase/arylesterase 1 OS=Homo sapiens GN=PON1 PE=1 SV=3	629	39902	6	21,1	202057	Green
71	PDLI7_HUMAN	Q9NR12	PDZ and LIM domain protein 7 OS=Homo sapiens GN=PDLIM7 PE=1 SV=1	1058	50928	11	22,1	192795	Green
72	RAB5B_HUMAN	P61020	Ras-related protein Rab-5B OS=Homo sapiens GN=RAB5B PE=1 SV=1	3515	23935	8	35,4	179196	Green
73	TLN1_HUMAN	Q9Y490	Talin-1 OS=Homo sapiens GN=TLN1 PE=1 SV=3	502	271935	38	18,3	175358	Green
74	ACTN4_HUMAN	O43707	Alpha-actinin-4 OS=Homo sapiens GN=ACTN4 PE=1 SV=2	589	105310	24	22,2	173469	Green
75	ENOA_HUMAN	P06733	Alpha-enolase OS=Homo sapiens GN=ENO1 PE=1 SV=2	783	47511	8	23,0	165945	Green
76	RSU1_HUMAN	Q15404	Ras suppressor protein 1 OS=Homo sapiens GN=RSU1 PE=1 SV=3	1377	31540	5	24,2	156746	Green
77	RAB5C_HUMAN	P51148	Ras-related protein Rab-5C OS=Homo sapiens GN=RAB5C PE=1 SV=2	1917	23711	9	43,5	155486	Green
78	CERU_HUMAN	P00450	Ceruloplasmin OS=Homo sapiens GN=CP PE=1 SV=1	503	123061	16	12,6	154660	Green
79	PGS1_HUMAN	P21810	Biglycan OS=Homo sapiens GN=BGN PE=1 SV=2	1067	42053	7	15,8	153733	Green
80	PLTP_HUMAN	P55058	Phospholipid transfer protein OS=Homo sapiens GN=PLTP PE=1 SV=1	832	54968	11	18,1	146646	Green
81	EHD2_HUMAN	Q9NZN4	EH domain-containing protein 2 OS=Homo sapiens GN=EHD2 PE=1 SV=2	1144	61333	8	19,9	145628	Green
82	KPYM_HUMAN	P14618-3	Isoform 3 of Pyruvate kinase PKM OS=Homo sapiens GN=PKM	850	56900	7	15,5	136216	Green

83	CNN1_HUMAN	P51911	Calponin-1 OS=Homo sapiens GN=CNN1 PE=1 SV=2	739	33342	8	42,8	129525	Green
84	PLSL_HUMAN	P13796	Plastin-2 OS=Homo sapiens GN=LCP1 PE=1 SV=6	435	70859	9	13,6	124837	Green
85	TAGL2_HUMAN	P37802	Transgelin-2 OS=Homo sapiens GN=TAGLN2 PE=1 SV=3	1525	22563	5	33,7	118009	Green
86	ANXA5_HUMAN	P08758	Annexin A5 OS=Homo sapiens GN=ANXA5 PE=1 SV=2	973	35994	9	34,7	116156	Green
87	C4BPA_HUMAN	P04003	C4b-binding protein alpha chain OS=Homo sapiens GN=C4BPA PE=1 SV=2	494	69086	6	12,2	115477	Green
88	RAB8B_HUMAN	Q92930	Ras-related protein Rab-8B OS=Homo sapiens GN=RAB8B PE=1 SV=2	3394	23755	10	40,6	102571	Green
89	EFHD1_HUMAN	Q9BUP0	EF-hand domain-containing protein D1 OS=Homo sapiens GN=EFHD1 PE=1 SV=1	1481	27042	9	40,2	102035	Green
90	TBB4A_HUMAN	P04350	Tubulin beta-4A chain OS=Homo sapiens GN=TUBB4A PE=1 SV=2	3229	50042	11	36,7	99380	Green
91	COF1_HUMAN	P23528	Cofilin-1 OS=Homo sapiens GN=CFL1 PE=1 SV=3	1596	18731	6	27,7	99303	Green
92	ANXA6_HUMAN	P08133	Annexin A6 OS=Homo sapiens GN=ANXA6 PE=1 SV=3	269	76216	12	20,8	78279	Green
93	IGHG4_HUMAN	P01861	Ig gamma-4 chain C region OS=Homo sapiens GN=IGHG4 PE=1 SV=1	3876	36454	7	23,6	73337	Green
94	ANXA4_HUMAN	P09525	Annexin A4 OS=Homo sapiens GN=ANXA4 PE=1 SV=4	950	36111	6	13,8	68210	Green
95	1433Z_HUMAN	P63104	14-3-3 protein zeta/delta OS=Homo sapiens GN=YWHAZ PE=1 SV=1	1133	27916	5	31,0	65901	Green
96	PRDX2_HUMAN	P32119	Peroxiredoxin-2 OS=Homo sapiens GN=PRDX2 PE=1 SV=5	389	22063	5	22,2	59102	Green
97	THRB_HUMAN	P00734	Prothrombin OS=Homo sapiens GN=F2 PE=1 SV=2	210	71520	9	10,1	55305	Green
98	1433E_HUMAN	P62258	14-3-3 protein epsilon OS=Homo sapiens GN=YWHAE PE=1 SV=1	934	29345	6	41,6	34207	Green
99	TBB4B_HUMAN	P68371	Tubulin beta-4B chain OS=Homo sapiens GN=TUBB4B PE=1 SV=1	3653	50287	12	40,5	33745	Green
100	TBB6_HUMAN	Q9BUF5	Tubulin beta-6 chain OS=Homo sapiens GN=TUBB6 PE=1 SV=1	2806	50313	8	29,2	31486	Green
101	RAB5A_HUMAN	P20339-2	Isoform 2 of Ras-related protein Rab-5A OS=Homo sapiens GN=RAB5A	1976	22349	9	55,7	29108	Green
102	HBG1_HUMAN	P69891	Hemoglobin subunit gamma-1 OS=Homo sapiens GN=HBG1 PE=1 SV=2	8137	16198	5	32,7	27489	Green
103	MYH14_HUMAN	Q7Z406	Myosin-14 OS=Homo sapiens GN=MYH14 PE=1 SV=2	1697	228840	27	14,6	4463	Green